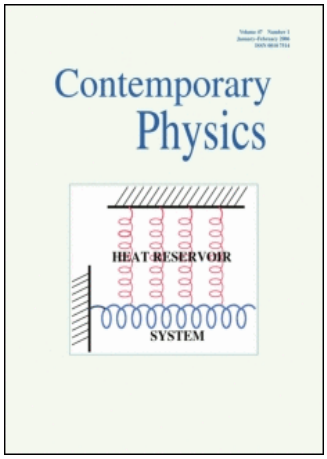

Contemporary Physics
Publication details, including instructions for authors and subscription information:
http://www.informaworld.com/smpp/title~content=t713394025

Environmental magnetism and climate change

Barbara A. Maher [a]
[a] Lancaster Environment Centre, University of Lancaster, Lancaster, UK

Online Publication Date: 01 September 2007
To cite this Article: Maher, Barbara A. (2007) 'Environmental magnetism and climate change', Contemporary Physics, 48:5, 247 - 274
To link to this article: DOI: 10.1080/00107510801889726
URL: http://dx.doi.org/10.1080/00107510801889726

Contemporary Physics, Vol. 48, No. 5, September – October 2007, 247 – 274

Environmental magnetism and climate change

BARBARA A. MAHER*

Lancaster Environment Centre, University of Lancaster, Lancaster, UK

(*Received 4 December 2007; in final form 17 December 2007*)

A major and pressing problem is to understand how, and how fast, the Earth's climate has changed in the past, with and without human influences on the global carbon cycle. Magnetic, remanence-acquiring, minerals, mostly iron oxides and sulphides, occur ubiquitously in sediments. They can act as sensitive recorders of past climates, because as climate has varied (from glacial to interglacial, for example), the mineralogy, magnetic domain state, composition and source of these minerals has varied. Here, the magnetic properties of windblown dust and interbedded soil layers of the Chinese Loess Plateau are used to calculate rainfall for the last million years, identifying the waxing and waning of the Southeast Asian summer monsoon. Comparison of our magnetic rainfall record on land with environmental records from the deep-sea shows that summer monsoon intensity is linked with growth and decay of continental-sized ice sheets, in turn reflecting changes in the Earth's orbit around the Sun.

1. Introduction

Climate change is a pressing global issue, with human-induced increases in atmospheric carbon dioxide and other greenhouse gases contributing a significant additional forcing mechanism in the global climate system. Improving our understanding of global climate processes becomes increasingly urgent as global warming progresses; knowledge of how the climate has changed in the past provides the critical context and perspective for both present understanding and future prediction of climate change. The defining feature of the current, Quaternary, geological period (which began around two million years ago and extends to the present day) is its large and numerous step changes in climate. These climate shifts have seen the build-up and decay of continent-sized ice sheets, major rises and falls ($\sim$120 m) in global sea level, and evolution, migrations and extinctions of fauna and flora, and large troughs and peaks (figure 1) in atmospheric CO_2 levels (e.g. $\sim$180 parts per million by volume (ppmv) in glacial stages and $\sim$280 ppmv in previous interglacial stages).

The present interglacial stage has lasted about 10,000 years, with atmospheric CO_2 values showing steepest rise in the last 200 years, to 385 ppmv at present and still rising. The peak of the last glacial stage was around 20,000 years ago and of the last interglacial, around 125,000 years ago (figure 1). These glacial/interglacial climatic and environmental shifts have imprinted themselves within natural sedimentary archives—layers of sediment laid down sequentially through time, in the ocean basins, in lakes, and as windblown dust on the continents, over timescales of up to $\sim$2 million years. These past climate imprints can comprise physical, chemical and isotopic variations within the sediments. If these proxy records can be retrieved and 'deciphered', information on the timing, rate and causes of climate change can be gained. Detailed and globally-distributed palaeoclimate records are needed, in order to test climate simulations (from climate models) and identify which areas or climate factors 'lead' in climate change (and may thus have causal significance) and which 'lag'. A major advantage of magnetic proxies of palaeoclimate is that they are sensitive, discriminatory, and also relatively fast, cheap and non-sample-destructive, enabling high-resolution retrieval of data through geological time and global space.

Here, the magnetic properties of natural materials are first outlined, and the six most common magnetic

*Corresponding author. Email: b.maher@lancs.ac.uk

Contemporary Physics
ISSN 0010-7514 print/ISSN 1366-5812 online © 2007 Taylor & Francis
http://www.tandf.co.uk/journals
DOI: 10.1080/00107510801889726

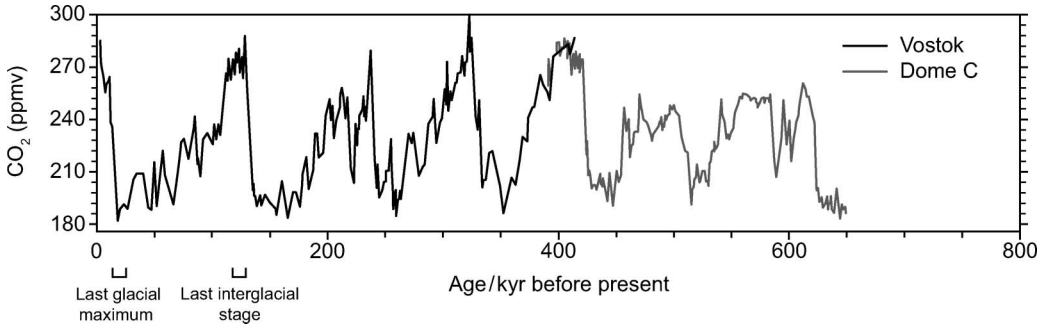

Figure 1. The record of atmospheric carbon dioxide over the past ~650,000 years, from gas bubbles in the Vostok ice core, Antarctica [1,2].

minerals that occur in natural materials identified and their origins discussed. The types of magnetic measurements routinely made to analyse and characterize environmental samples, and the instrumentation required, are also outlined. The application of magnetic methods to climate reconstruction is then discussed, using the example of the Chinese loess and palaeosols, which together make up a vast wedge of sediment that records changing monsoonal rainfall through the last 2.5 million years. Finally, some future likely developments and applications of environmental magnetism to new studies of climate change are identified.

2. Magnetism of natural materials

2.1 Magnetic minerals

Magnetism is a fundamental property of all materials. Materials respond to being placed in a magnetic field by producing magnetic fields of their own and some generate magnetic fields spontaneously, without application of any external field. All magnetic fields are generated by electric currents. At the atomic level, magnetic fields arise from the spin of electrons about their own 'axes' and their orbital motion within different energy levels about their central nucleus. These moving charges, which can be thought of as describing tiny current loops (figure 2(*a*)–(*d*)), are acting as magnetic moments (*m*). If any material is subjected to an applied magnetic field, $\boldsymbol{H}$, these magnetic moments will respond and give rise to an induced magnetization ($\boldsymbol{M}_i$, the magnetic moment per unit volume, ampere/metre, or per unit mass, A m^2 kg^{-1}). The relationship between the induced magnetization and the applied external field is

$$\boldsymbol{M}_i = \boldsymbol{K}\boldsymbol{H} \quad \text{or} \quad \chi\boldsymbol{H}.$$

The parameter, $\boldsymbol{K}$ or χ, is known as the magnetic susceptibility; it is often treated as a scalar but can be a complicated function depending on factors including temperature, crystal shape, crystal defects and stress, and frequency of the applied field/timescale of measurement (see frequency dependent susceptibility below). The volumetric magnetic susceptibility (K) is dimensionless; the mass susceptibility, $\chi = K/\rho$ (where ρ is the density), is also used, in units of m^3 kg^{-1}.

For moderately detailed classical and/or quantum mechanical treatments of magnetism and material magnetic properties, the reader is referred to, for example, Jiles [4], and, in the context of palaeomagnetic studies, to Tauxe [3] and Butler [5]. Figure 3 shows the three basic types of magnetic response observed when $\boldsymbol{M}_i$ is monitored upon application of a magnetic field, $\boldsymbol{H}$. In diamagnetic materials (figure 3(*a*)), the response to an applied magnetic field is to acquire a small induced magnetization, opposite to the direction of the applied field. This results from the torque exerted on the orbital motion of the electrons by the applied magnetic field, which causes the moments to precess and create a current about an axis parallel to the applied field. This induced current creates a weak magnetic field opposing $\boldsymbol{H}$. In diamagnets, the electron spin magnetic moments make no contribution to the magnetization because they are paired and cancel each other out. The magnetization depends linearly on the field—i.e. the diamagnetic susceptibility is negative and constant—and diminishes to zero upon removal of the field. Diamagnetic susceptibility is essentially temperature-independent. Natural materials displaying diamagnetic behaviour include quartz, silica and water, a typical diamagnetic susceptibility value being $\sim -8 \times 10^{-8}$ m^3 kg^{-1}.

Diamagnetism is a property of all matter but is most often swamped by other, stronger magnetic effects whenever there are atoms with net, i.e. non-cancelled, magnetic moments, arising from the presence of unpaired electron spin moments. Before the application of an external field, these permanent magnetic dipoles are randomly orientated due to thermal agitation. Upon application of a field, they tend to align themselves parallel with the field direction, resulting in a weak, positive induced magnetization

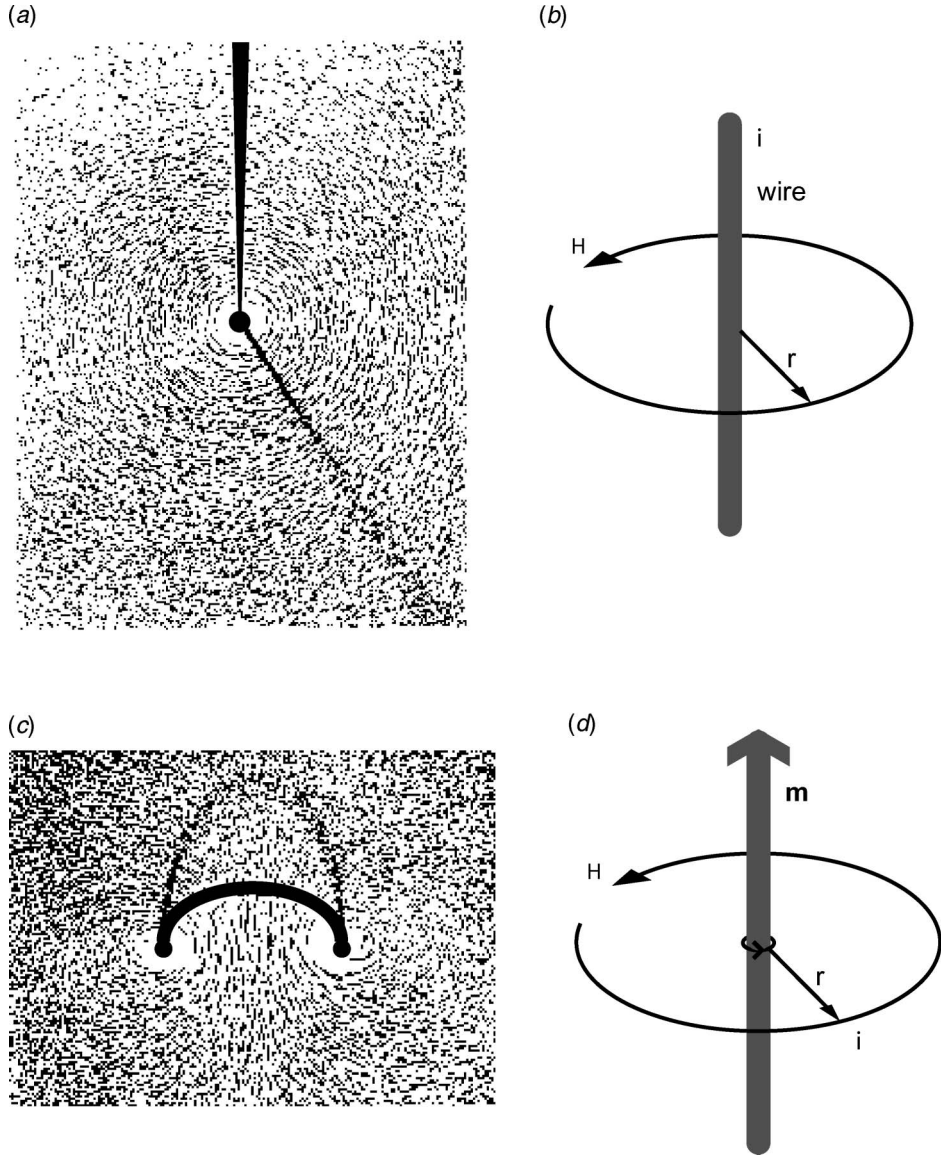

Figure 2. (*a*) The pattern taken up by iron filings sprinkled on a flat sheet pierced by a wire carrying a current i (adapted from Jiles, 1998 and [3]). The circular pattern results from the filings lining up with the magnetic field produced by the current in the wire; (*b*) the relationship of magnetic field, $\boldsymbol{H}$, to current, i, for a length of straight wire (from [3]). The magnitude of the field, H, is proportional to the strength of the current i. In this case, the magnitude of H (in units of A m^{-1}) is given by Ampère's law: $H = i/2\pi r$; (*c*) as shown in (*a*), an electrical current in a wire produces a magnetic field which curls around the wire. If the wire carrying a current, i, is bent into a loop with area r^2, the current loop creates the magnetic field shown by the iron filings; (*d*) this magnetic field is the same as that which is produced by a magnet with a magnetic moment $\boldsymbol{m}$. This moment is created by the current i and also varies with the area of the current loop (the bigger the loop, the bigger the moment), hence $\boldsymbol{m} = i\pi r^2$.

(figure 3(*b*)). Upon removal from the field, the magnetization returns to zero as the weak magnetic ordering is broken down by thermal effects. Thus, paramagnetic susceptibility is positive, weak (but greater than diamagnetism) and inversely proportional to temperature. Many natural iron- and manganese-containing minerals are paramagnetic at Earth surface temperatures, including biotite, with a susceptibility value of $\sim 80 \times 10^{-8}$ m^3 kg^{-1}, pyroxene ($\sim 50 \times 10^{-8}$ m^3 kg^{-1}) and the iron oxyhydroxide, lepidocrocite ($\sim 70 \times 10^{-8}$ m^3 kg^{-1}).

In contrast with the weak magnetizations associated with diamagnets and paramagnets, there is a third category of

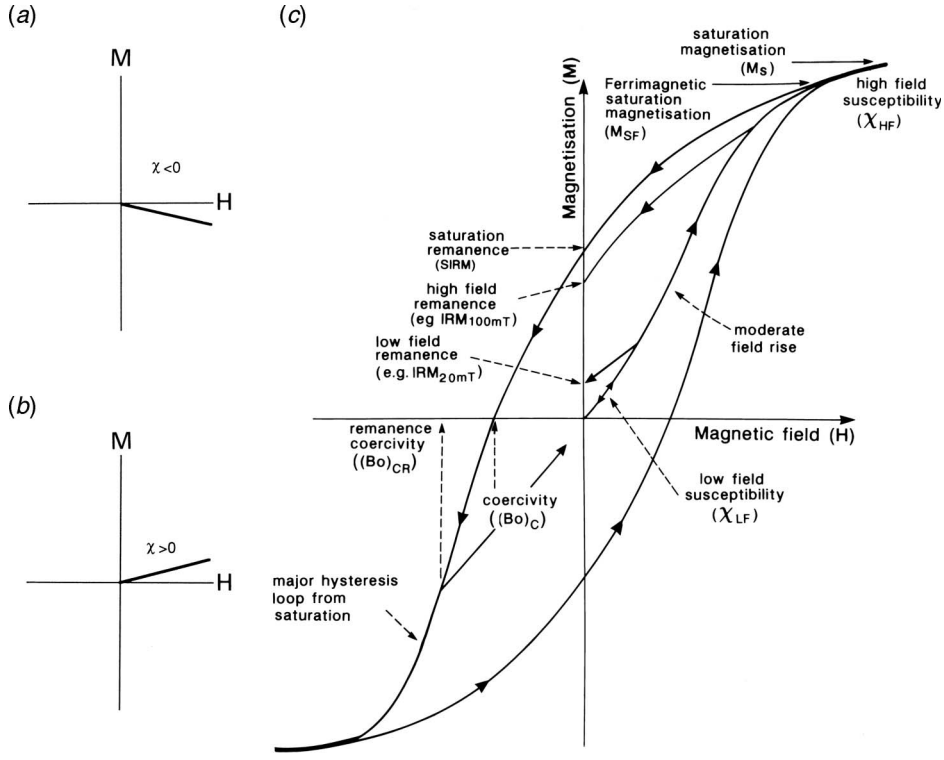

Figure 3. (*a*) Diamagnetic response to an applied field; (*b*) paramagnetic response; (*c*) ferromagnetic response (from [5] and [7]).

magnetic response which exhibits strong and spontaneous magnetizations (i.e. even in the absence of any external field), and magnetic remanence-carrying capability (figure 3(*c*)). Due to their crystal structures and density of packing, ferromagnetic materials have strong positive exchange interactions between their neighbouring atomic magnetic moments. The result of these couplings is to produce spontaneous magnetizations and large induced magnetizations, which resist thermal disturbance and are orders of magnitude greater than for their paramagnetic counterparts in the same magnetizing field. As can be seen from figure 3(*c*), ferromagnets show steep increases in magnetization with applied field, until reaching saturation magnetization (SIRM); they display hysteresis (i.e. magnetization lags the applied field and is irreversible); magnetic susceptibility is not a simple constant. The magnetic coupling produced by exchange interactions can have different configurations (figure 4). Ferromagnets have entirely parallel alignment between coupled magnetic moments; antiferromagnets have (as their name suggests) anti-parallel coupling; ferrimagnets have opposite but unequal magnetic coupling. Upon heating and thermal expansion, the strength of exchange coupling and resultant magnetization decrease. Ferro- and ferrimagnets each have a characteristic temperature, the Curie point, at and above which exchange interaction is (reversibly) prevented and

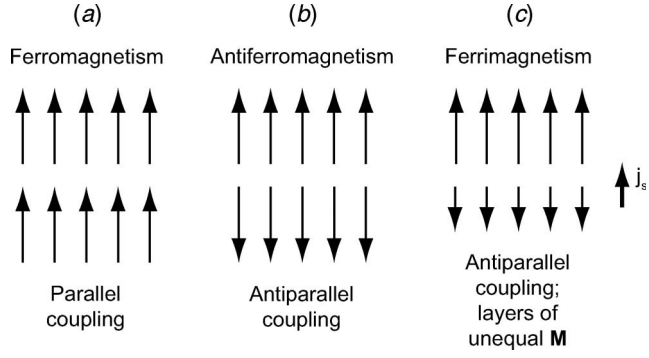

Figure 4. Exchange coupling for (*a*) ferromagnets, (*b*) antiferromagnets, (*c*) ferrimagnets (from [6] and [5]).

they become paramagnetic ($\sim$770°C for iron, 580°C for magnetite). Iron, a ferromagnet, has an initial, reversible, low-field susceptibility of $\sim 200\ 000 \times 10^{-8}$ m^3 kg^{-1}, magnetite, a ferrimagnet, $\sim 60\ 000 \times 10^{-8}$ m^3 kg^{-1}.

The magnetic properties of most natural environmental samples dominantly reflect the presence of one or more of the following six mineral types: the iron oxides, magnetite (Fe_3O_4), maghemite (γFe_2O_3), and haematite (αFe_2O_3); the iron oxyhydroxide, goethite (αFeOOH); and the iron

sulphides, greigite (Fe_3S_4), and pyrrhotite ($Fe_7S_8 - Fe_{11}S_{12}$). All of these minerals display strong magnetic characteristics and are capable of carrying a magnetic remanence at room temperature. An oxide structure is made up of a lattice of close-packed oxygen anions, incorporating a number of interstices which are able to accommodate metallic cations. In the iron oxides, Fe^{2+} and Fe^{3+} cations are the major interstitial occupants, but both cation-deficient and isomorphously substituted structures can also exist. For example, solid solution series exist between magnetite and ulvospinel ($FeTiO_4$), and haematite and ilmenite ($FeTiO_3$), with gradual changes in the magnetic properties from one end-member composition to the other, and between magnetite and maghemite. Magnetite has the crystal structure of an inverse spinel and is ferrimagnetic (figure 5, and see http://webmineral.com/data/Magnetite.shtml). Present within the cubic close-packed oxygen of the spinel structure are two different interstitial sites, the A and B sites. The A site is surrounded by 4 oxygen ions forming a tetrahedral cell, the B site by 6 oxygen ions forming an octahedral cell. The unit cell (i.e. the basic repeated structural block) of magnetite contains 32 oxygen ions and 24 Fe sites, of which 8 are A sites and 16 are B sites. In stoichiometric magnetite, all 24 Fe sites are occupied, with the 8 A sites hosting 8 Fe^{3+} cations and the B sites a mix of the 8 remaining Fe^{3+} cations together with the 8 Fe^{2+} cations. This structure displays ferrimagnetism due to (a) exchange interactions, and (b) the unbalanced antiparallelism of the magnetic moments generated by the A site (8 Fe^{3+}) and B site cations (8 $Fe^{3+} + 8$ Fe^{2+}).

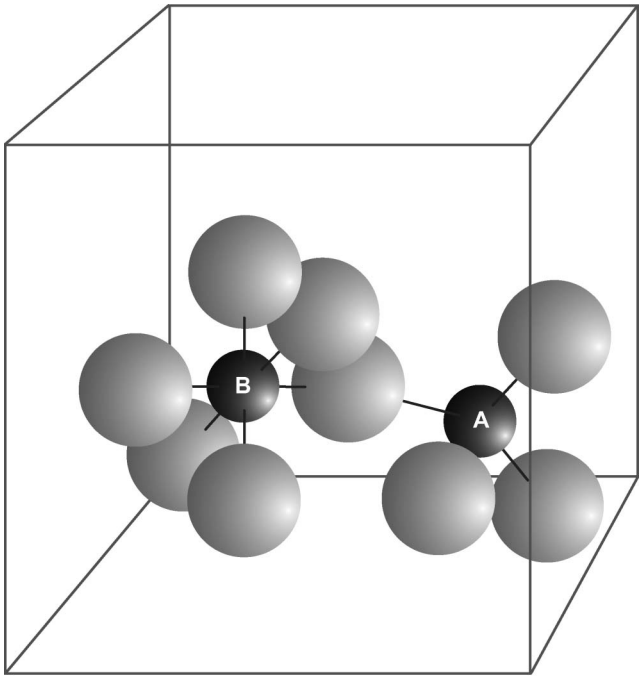

A = A sublattice Fe cation, surrounded by 4 oxygen anions
B = B sublattice Fe cation, surrounded by 6 oxygen anions

Figure 5. Crystal structure for magnetite, Fe_3O_4 (from [5]).

2.2 Magnetic minerals in sediments

Magnetite is the strongest magnetic mineral found in environmental samples (susceptibility $\sim 50 - 60\,000 \times 10^{-8}$ m^3 kg^{-1}, SIRM $\sim 10 - 20$ A m^2 kg^{-1}). Maghemite (γFe_2O_3) nicely demonstrates the distinction between compositional and structural contributions to mineral magnetic behaviour, as it has the same composition as haematite (αFe_2O_3) but the structure of a spinel. Maghemite is thus a ferrimagnet (with very similar magnetic properties to magnetite), whereas haematite is 'almost antiferromagnetic' (see below). Maghemite is a cation-deficient spinel, lacking sufficient Fe^{+3} ions to fill the available Fe sites. It is metastable with respect to haematite (it inverts to haematite upon heating) but can be stabilized by the presence of Al ions (one of the most commonly available metal cations in soils) substituting within some of the vacant sites. Titanium-substituted magnetites and maghemites, formed at high temperatures in igneous settings, have been the traditional focus of study by geophysicists concerned with palaeomagnetic studies of, for example, sea-floor spreading and marine magnetic anomalies (figure 6). Because these minerals form at high temperatures and then cool through their Curie points, they acquire a permanent magnetization aligned with the direction of the Earth's magnetic field at their time of cooling. Until recently (the last ~ 30 years), it was thought that magnetite could only form in igneous rock-forming environments. However, environmental magnetic studies have revealed that a range of ferrimagnetic minerals can be formed at Earth surface temperatures and pressures within soils and sediments, rather than merely 'inherited' from disintegration and weathering of magnetic mineral-bearing igneous rocks. Notably, trace concentrations of nanoscale magnetite can be precipitated *in situ* in the soil matrix of well-drained, generally oxidizing, near-neutral soils (figure 7; [8 – 10]). Further, nanoscale magnetite and greigite crystals can be actively formed within the cells of magnetotactic bacteria (figure 8), forming chains of biologically-controlled crystals, some of which demonstrate unique crystal shapes (figure 9), which efficiently align the bacterial cell with the Earth's magnetic field [11,13]. Upon death of the bacteria, these intracellular, biologically-organized magnetic minerals may be preserved in the sedimentary record. Ferrimagnets can also form in soils through the effects of forest and grassland fires, through the combined effects of heating, dehydration and a reducing soil pore atmosphere, due to burning of vegetation. Finally (so far!), ferrimagnets can also form and be released into

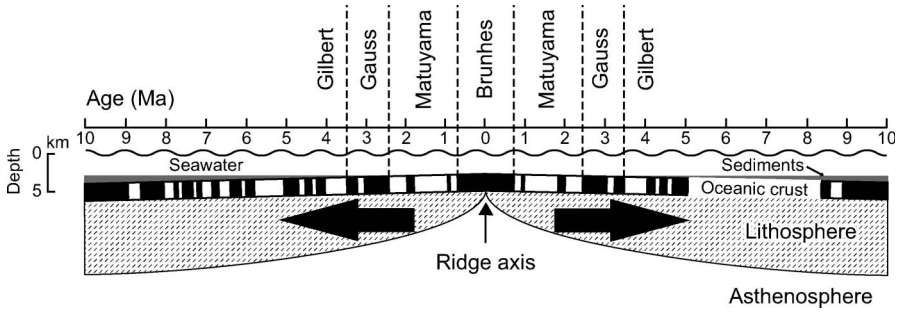

Figure 6. Marine magnetic anomalies in oceanic crust, reflecting sea floor spreading at this mid-ocean ridge and successive recording of normal and reversed magnetic polarity through time as new crust is created. The absolute age of the crust is given by the horizontal scale and the geomagnetic polarity epochs (Brunhes, Matuyama etc. also noted from [5]).

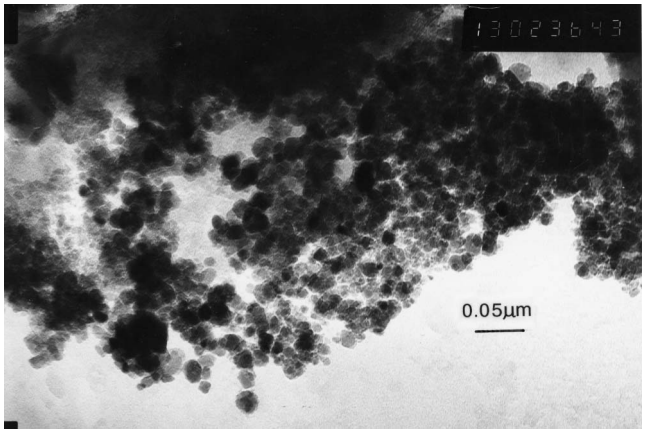

Figure 7. Transmission electron micrograph of soil-formed (pedogenic) submicrometre magnetite crystals, from an unburnt, well-drained, near-neutral soil, Exmoor, UK [8].

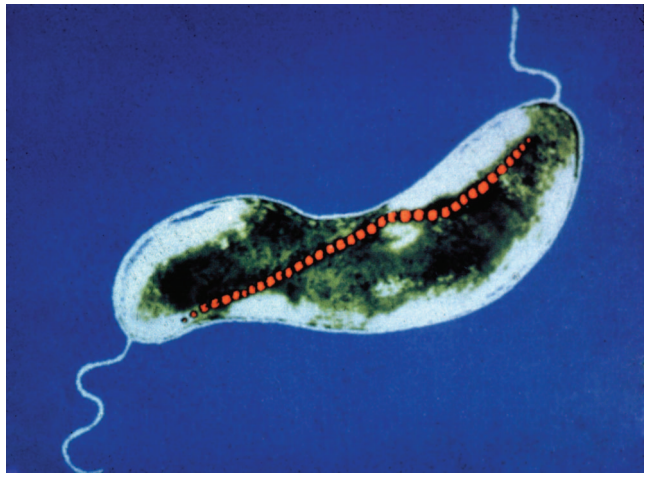

Figure 8. False colour transmission electron micrograph, a magnetotactic bacterium, with its intracellular chain of magnetite crystals (photo by H. Vali), reproduced with permission from *Nature*, **343**, 213. Copyright 1990, MacMillan Magazines Ltd.

the atmosphere anthropogenically through combustion of fossil fuels, due to the presence of iron impurities within the fuel (figure 10; [14,15]).

The most oxidized iron compound, haematite, has an oxygen lattice of hexagonal close packing, forming a rhombohedral structure consisting of offset, stacked layers of triplets of oxygen ions with Fe^{3+} cations on either side (figure 11, and see http://webmineral.com/data/Hematite.shtml). Here, the superexchange coupling of the Fe^{3+} cations in each of the $Fe-O_3-Fe$ triplets is negative, so that each of the magnetic moments is oppositely aligned. Haematite is thus basically antiferromagnetic in structure. However, haematite samples often do not behave as perfect antiferromagnets; instead, they display weak but stable magnetic remanence (SIRM ~ 0.25 A m^2 kg^{-1}) and significant positive susceptibility ($\sim 60 \times 10^{-8}$ m^3 kg^{-1}). Two possible reasons for this imperfect antiferromagnetism are a degree of misalignment of the negatively coupled spins (spin canting), leading to imperfect cancelling, and/or a weak, parasitic ferromagnetism arising from crystal defects. The Néel point (the equivalent of the Curie point in ferro/ferrimagnets) of haematite is $\sim 685°C$. The iron oxyhydroxide, goethite, shares similar magnetic characteristics to haematite, with weak but even more stable magnetization (SIRM ~ 0.05 A m^2 kg^{-1}, susceptibility $\sim 70 \times 10^{-8}$ m^3 kg^{-1}). Its Fe^{3+} ions occupy the centre of a distorted octahedral cell of oxygen and hydroxyl anions, within an orthorhombic structure. As for haematite, the Fe^{3+} cations are negatively coupled, with weak defect ferromagnetism due to ordered defects. In terms of absolute concentration, haematite and goethite occur as the most important iron oxides within soils; rather than occurring as trace minerals, like magnetite and maghemite, they can be detected by x-ray diffraction of whole soil samples, at concentrations of $\sim 5-10\%$. They precipitate within

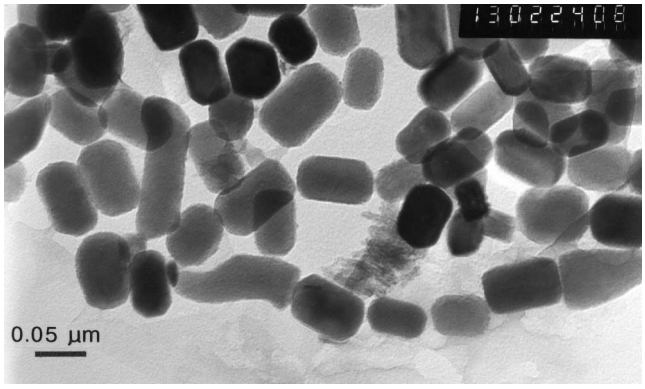

Figure 9. Transmission electron micrograph of unique crystal morphologies (bullets and clogs) for bacterial magnetites (photo by M. Hounslow from [7]). Copyright 1999. Reprinted with permission by Cambridge University Press.

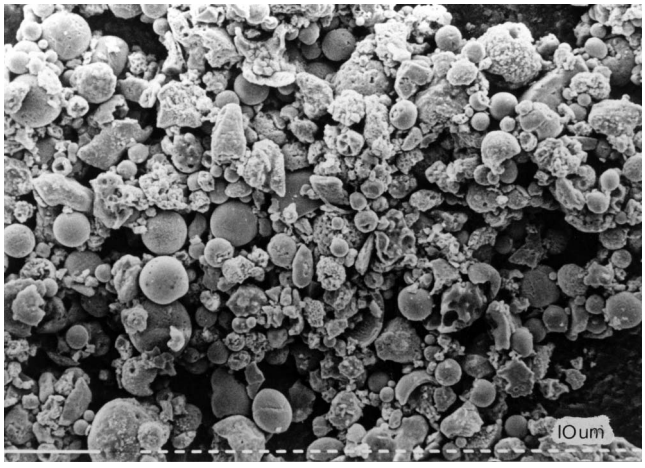

Figure 10. Scanning electron micrograph of anthropogenically-produced magnetic spherules, pollution particles formed by combustion of fossil fuels containing iron as a non-volatile impurity (photo by A. Hunt from [7]). Copyright 1999. Reprinted with permission by Cambridge University Press.

oxidizing soil micro-environments, upon oxidation of Fe^{2+} cations released from primary Fe-bearing minerals by weathering processes.

The iron sulphides, greigite and pyrhhotite, are ferrimagnetic, with susceptibility values of ~ 120 and 50×10^{-8} m^3 kg^{-1}, respectively, and distinctively high SIRM/χ ratios [16,17]. These minerals only form in reducing (anaerobic) environments, such as estuarine muds, where organic matter has been consumed by bacteria in the absence of oxygen.

For this key group of ferrimagnets and imperfect antiferromagnets, the presence of magnetic domains cause the initial susceptibility and a range of magnetic remanence

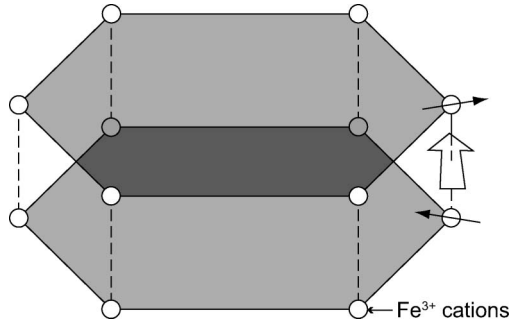

Figure 11. Crystal structure of haematite, with parallel magnetic moments from the Fe^{3+} cations within any one basal (0001) plane and coupling of magnetic moments between planes. The vector sum of the nearly antiparallel moments is indicated by the white arrow (from [5]).

properties to be grain size-dependent (figure 12). Grain size exerts no intrinsic control on magnetization; rather, the measured magnetic properties are influenced by the magnetic domain state of the sample's magnetic minerals. Domain state in turn is a function of grain size. Magnetic domains are regions within a crystal, often around a few hundreds of nanometres diameter, with uniform directions of magnetization, i.e. where the magnetic moments are aligned with each other. Magnetic domains are separated from each other by domain walls ($\sim 5-200$ nm thickness), within which the direction of magnetization changes from that of one domain to that of the neighbouring domain. Magnetic domains form because they produce a lower total energy state for the magnetic grain. A ferrimagnet with spontaneous magnetization can exist in a demagnetized state by having a number of domains each magnetized in different directions, so that the net magnetization of the grain is zero. Domains cannot form in critically small grains, where the grain volume is insufficient to contain a domain wall. Domain-transition/grain size thresholds vary with temperature, mineral composition and microstructure. At room temperature, magnetite particles with grain sizes in the range of $\sim 0.030-0.070$ μm are single domain while grains in the size range ~ 0.07 to ~ 2 μm are pseudosingle domain. Single domain grains carry the most stable remanent magnetizations. The only way to change the magnetization of a single domain grain is to rotate its magnetization, an energetically difficult process. Larger, multidomain (MD) grains ($> \sim 2$ μm) have significantly weaker magnetizations and lower magnetic stability than single domain and pseudo-single domain particles. To magnetize a multidomain grain, the domain walls need to be moved, an energetically easy process. Lowest magnetic stability is shown by superparamagnetic (SP) particles, typically $< \sim 30$ nm in magnetite, in which thermal energy is dominant over magnetic energy, so that the moments are constantly disordered and

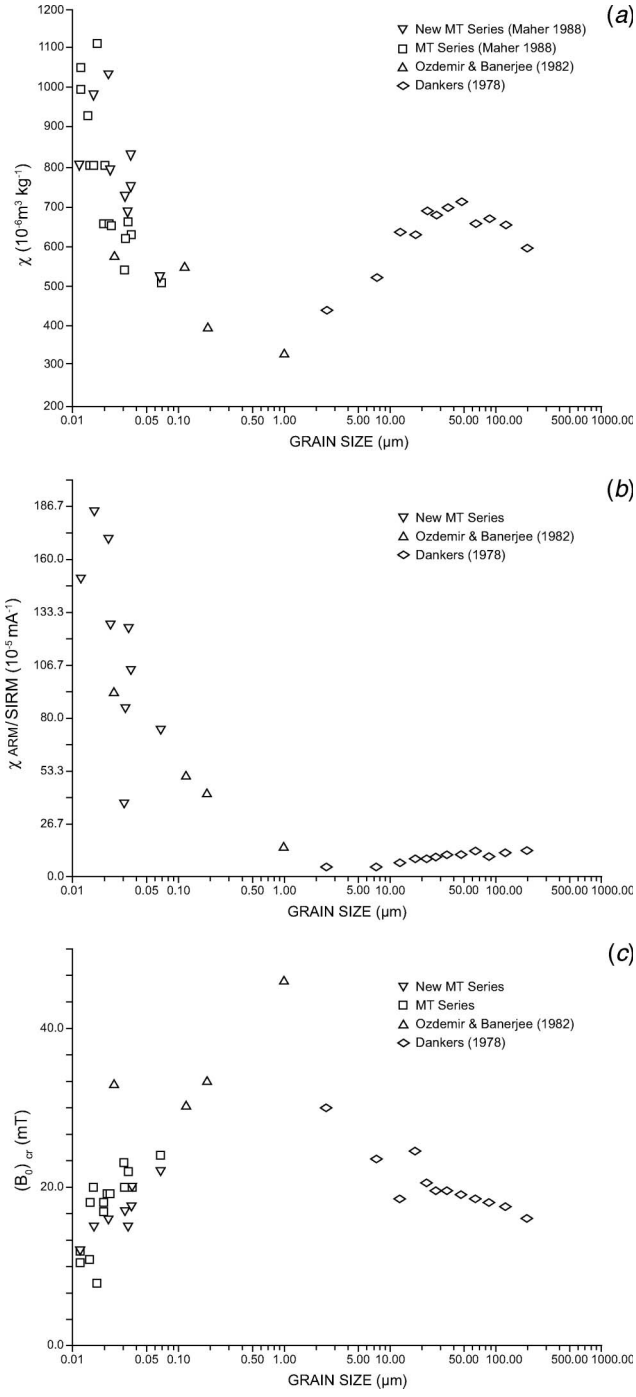

Figure 12. Grain size dependence of (*a*) initial, low field susceptibility; (*b*) the ratio of anhysteretic magnetization (ARM, expressed as susceptibility of ARM, having normalized by the biasing field) and saturation magnetization (SIRM); (*c*) coercivity of remanence (i.e. the dc field required to demagnetize an SIRM back to zero).

they carry no magnetic remanence. They do, however, have a significant susceptibility. In low fields (depending on their frequency, see below), there is net alignment of their $\sim 10^5$ atomic magnetic moments with the magnetic field; hence, they behave like 'strong' paramagnets (hence their name). Figure 12(*a*)–(*c*) summarize the grain size dependence of some routinely measured magnetic parameters in sized, pure magnetite powders.

3. Sample characterization

Similar to the concept of magnetic non-destructive evaluation for testing of engineering materials, we can cycle our environmental samples round full or partial hysteresis loops, in order to analyse and characterize their magnetic properties. For magnetic measurements, there are three magnetic units of concern: one for field ($\boldsymbol{H}$ or $\boldsymbol{B}_0$), one for magnetization ($\boldsymbol{M}$) and one for susceptibility ($\boldsymbol{K}$). Unfortunately, several sets of unit systems have been commonly used in magnetic studies, leading to possible confusion. As outlined by Maher and Thompson [7], magnetic induction ($\boldsymbol{B}$), magnetic field ($\boldsymbol{H}$) and magnetization ($\boldsymbol{M}$) are related in SI units by the vector equation

$$\boldsymbol{B} = \mu_0(\boldsymbol{H} + \boldsymbol{M}),$$

where μ_0 ($=4\pi \times 10^{-7}$ ohm-seconds per metre) is a physical constant, the permeability of free space. In environmental magnetism, most studies tend to express results in terms of field, expressed in Tesla, rather than induction. $\boldsymbol{B}$ (induction) is replaced by field, $\boldsymbol{B}_0$, via the 'free space induction' ($=\mu_0\boldsymbol{H}$). Alternatively, field measurements can be expressed in terms of $\boldsymbol{H}$, in units of ampere per metre.

Magnetization ($\boldsymbol{M}$) is defined as the magnetic moment per unit volume, measured in ampere/metre (A m^{-1}). Magnetic susceptibility (as above) relates $\boldsymbol{M}$ and $\boldsymbol{H}$ by the equation $\boldsymbol{M}=\boldsymbol{k}\boldsymbol{H}$, indicating the 'magnetizability' of a material when subjected to a magnetic field. $\boldsymbol{M}$ and $\boldsymbol{H}$ have the same units so $\boldsymbol{k}$ is dimensionless. For characterizing environmental samples, it is more common to report magnetic properties per unit mass of sample measured rather than unit volume, giving initial low-field susceptibility, χ, in units of $m^3\ kg^{-1}$ and remanent magnetizations in units of A $m^2\ kg^{-1}$.

For environmental magnetic studies, dealing with natural samples containing distinctive and different magnetic minerals, a relatively small number of magnetic parameters can often be measured which provide sufficient grain size- and composition-related magnetic mineral information to identify the key magnetic components and/or achieve a discriminatory magnetic 'signature' for each sample. Figure 13 and table 1 summarize the magnetic parameters used routinely in exploring the magnetic mineralogy of environmental materials. For the mixtures of ferrimagnetic, imperfect antiferromagnetic and paramagnetic minerals typically found in most environmental materials, the shape

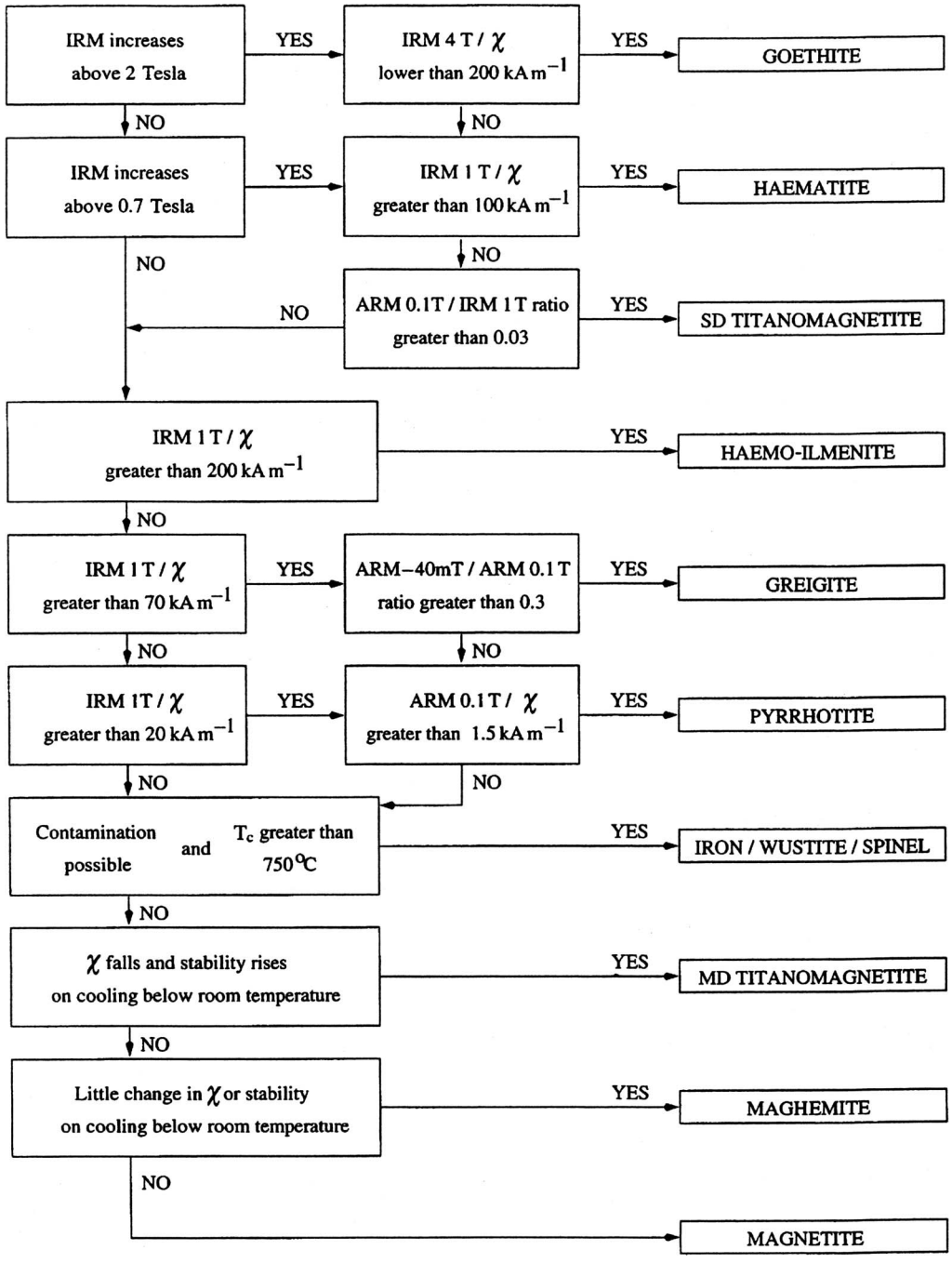

Figure 13. Flow chart of routine, diagnostic magnetic measurements (from [7]).

of the magnetization curve shown in figure 3(*c*) resembles an S shape. As the applied field is raised slightly from zero, the resulting induced magnetization rises linearly from the origin; upon removal of this small field (typically, for initial susceptibility measurements, a field of $\sim$0.1 mT, around twice the Earth's magnetic field, is used), the magnetization reduces to zero. This reversible magnetization response reflects the combined response of the constituent magnetic grains, especially the ferrimagnets. In any multidomain grains, some reversible movement of the domain walls will have occurred, causing enlargement of those domains with moments aligned closest to the direction of the applied field, together with some slight rotation of the non-aligned moments. Single domain grains will have rotated slightly towards the field direction. Superparamagnetic grains will have taken on a net statistical alignment with the field.

Table 1. Summary of typical magnetic properties of natural minerals (from [7]).

Mineral	T_c (°C)	M_s (A m^2 kg^{-1})	χ (10^{-6} m^3 kg^{-1})	ARM (mA m^2 kg^{-1})	SIRM (A m^2 kg^{-1})
Magnetite (soft)	575	92	560	18	9
Magnetite (hard)	575	92	400	110	22
Titanomagnetite (soft)	200	24	170	80	7
Titanomagnetite (hard)	200	24	200	480	12
Haematite	675	0.5	0.6	0.002	0.24
Goethite	150	0.5	0.7	0.005	0.05
Greigite	300	20	120	120	11
Pyrrhotite	300	17	50	50	4.5
Iron	770	220	2000	800	80
Paramagnet	$1/T$	–	~ 1	0	0
Diamagnet	constant	–	-0.006	0	0

T_c = Curie temperature or thermomagnetic behaviour; M_s = saturation magnetization; χ = initial AC susceptibility; ARM = anhysteretic remanence imparted in a 100 mT peak alternating field with a dc biasing field of 0.1 mT; SIRM = isothermal remanence imparted in a 1 T dc field.

Upon removal of the field, the grains return to their 'pre-magnetized' state. If the applied field is then increased, magnetization again increases but this time nonlinearly and non-reversibly. When the applied field is removed, the induced magnetization does not return to zero but instead relaxes to a remanent magnetization. This irreversible magnetization reflects irreversible domain wall movements in multidomain grains and rotation of the previous easy axes of magnetization in single domain grains. Superparamagnetic grains do not contribute to the remanence, due to rapid thermal disordering of any previous in-field alignment. Further increases in applied field intensity continue to induce increased in-field and remanent magnetization, until a point is reached when no further in-field magnetization can be induced despite any continued field increase. This point represents the saturation magnetization, when there is maximum alignment of the multidomain domains and the individual single domain grains have all been rotated with the field direction. This saturation magnetization relaxes, upon removal of the field, to the saturation remanence (SIRM). Magnetization loss from the saturation magnetization (M_s, see figure 3(c)) to the saturation remanence tends to be highest in multidomain and least for single domain grains. For an assemblage of randomly orientated, non-interacting single domain magnetite grains, the M_s/SIRM ratio is ~ 0.5; for pseudo-single domain grains, between 0.1 and 0.3; for multidomain grains, less than 0.1; for superparamagnetic grains, less than 0.1 (tending towards zero). The slope at the tip of the M/H loop (the high-field susceptibility, χ_{hf}) is dominated by the paramagnetic contribution. If, having attained saturation of the sample, a series of fields is then applied in an opposite direction, the demagnetization behaviour of the assemblage can be identified. Due to their higher magnetic stability and remanence, single domain magnetites have wider loops than multidomain particles. The field required to reduce the M_s to zero is the coercive force; that required to reduce the SIRM to zero is the coercivity (figure 3(c)). Upon further increases of the applied field, the magnetization continues to change rapidly before again slowing and approaching saturation at the lower left tip of the hysteresis loop. Various 'low-field' and 'high-field' remanence ratios are also shown in figure 3(c). Remanence ratios ($IRM_{n\ mT}$/SIRM) are often used in environmental magnetic studies to characterize the stability of samples. For example, the 'high-field remanence' (HIRM) is often used to identify the relative contribution of harder magnetic minerals, such as haematite, to the sample remanence. In the case of many magnetic laboratories, the maximum dc field available for remanence acquisition has been of the order of 1 Tesla (T). The 'HIRM' has thus often been reported as the remanence acquired between either 100 milliTesla (mT) or 300 mT and the 'saturating' field of 1 T. However, it should be noted that partially oxidized magnetite can acquire significant IRM in fields in excess of 300 mT, while samples of goethite and haematite continue to acquire magnetization even in applied fields as high as 7 T [18,19]. However, even when the maximum dc field available is ~ 1 T, the remanence acquisition and demagnetization behaviour of goethites, haematites and maghemitized magnetites is distinctive. The response of each mineral to alternating field demagnetization (with a peak field of ~ 100 mT) of the resultant high-field remanence appears diagnostic. Irrespective of their grain size, the goethites retain most ($\sim 90\%$) of their HIRM; for the haematites, the HIRM loss is as much as $\sim 25\%$; while the softest, maghemite sample relinquishes virtually all ($\sim 99\%$) of its HIRM. Thus, the mass-normalized $HIRM_{1\ T\ (100\ mT\ af)}$ may provide the simplest means of estimating the remanence contributed by the high-coercivity minerals.

An anhysteretic (i.e. hysteresis-free) remanent magnetization (ARM) is an additional key magnetic property. It is

produced by cycling the magnetization around progressively smaller hysteresis loops, by gradually reducing the amplitude of an alternating magnetic field, whilst superimposing a small steady field. ARMs are particularly useful in identifying magnetic grain size changes between samples (figure 12(*b*)) and/or the effects of magnetic interactions [20,21].

Finally, another routinely used magnetic measurement is the frequency dependence of initial, low field susceptibility (χ_{FD}). Initial, low field susceptibility is dependent on the frequency at which it is measured, because susceptibility depends on the magnetic domain state of the sample being measured. In turn, domain state depends on the length of time over which the sample is being measured. Frequency dependent susceptibility is often defined as the change in susceptibility when measured at low frequency ($\sim$500 Hz, χ_{LF}) and high frequency ($\sim$5000 Hz, χ_{HF}). Over this change in frequency, there is a narrow interval of ferrimagnetic grain sizes ($\sim$0.02 μm in magnetite) which will be superparamagnetic at the low frequency of measurement but single domain at the higher frequency of measurement. Over the longer measurement period at 470 Hz, such grains will show net alignment with the field, contributing their many individual magnetic moments to the susceptibility. Over the shorter measurement times, at 4700 Hz, they will 'block in' (i.e. their relaxation times will exceed the experimental measurement time) and behave as single domain grains, with a much lower susceptibility. For superparamagnetic grains, the decrease in susceptibility per decade of frequency is up to $\sim$18%, compared with $<$1% for single domain and multidomain grains.

In addition to these routinely used hysteresis and remanence measurements, smaller subsets of representative samples can be analysed in more detail, to identify changes in magnetization not only with field, but with temperature (high or low), time, stress, and rotation. In particular, Curie points and crystallographic transition temperatures can provide sensitive discrimination between the magnetic mineralogies of natural samples. The presence of organic matter within many natural materials often precludes high-temperature measurements. Irreversible changes in magnetic mineralogy can result from unwanted experimental exposure to reducing conditions upon release of carbon monoxide from combustion of such material.

4. Instrumentation

Four laboratory instruments make up the basic requirements for magnetic characterization of environmental samples: a susceptibility bridge (preferably dual frequency); a magnetometer; magnetizing coils; and a demagnetizer. With the exception of the demagnetizer, these instruments are readily and relatively cheaply available in rugged and portable form. Susceptibility bridges such as the widely used Bartington system contain an inductor, which, together with a capacitor and a current-controlled oscillator, creates a low-frequency alternating magnetic field at frequencies of $\sim$0.5 kHz and $\sim$5 kHz, and an AF intensity of 80 A m^{-1} (= 0.1 mT). Introducing a sample into this field produces a detected change in frequency of oscillation. Calibration is achieved using paramagnetic salts. For very weakly magnetic samples, correction may need to be made for the diamagnetic susceptibility of the sample holder and any sample packing materials. For generating incrementally increasing laboratory applied fields, pulse magnetizers are effective, producing uniform, repeatable fields of up to $\sim$4 T in a few seconds by discharge of energy stored in a capacitor bank into a solenoid. Iron-cored electromagnets can also be used to generate peak dc fields of $\sim$1 T but are slower to charge and discharge, and can produce inadvertent demagnetization due to stray fields around the electromagnet. For calibration, Hall effect probes can be used to measure and intercalibrate steady, pulsed and alternating current fields between $\sim$3 mT and 3 T, encompassing the main range of requirement for environmental studies. As with susceptibility bridges, magnetometers for measuring environmental samples have to be able to measure magnetizations that vary over a very large range (e.g. by a factor of up to 10^6). Fluxgate magnetometers are reliable, sensitive, and can typically measure magnetizations from between 10^{-7} to 10^{-2} A m^2. Portable, battery-operated versions of this instrument can be readily carried to any laboratory or field site. Calibration needs careful monitoring, to avoid undue drift, most often using a small strip of magnetic tape or a rock sample cross-calibrated to an independent SQUID or astatic magnetometer. The calibration samples themselves need to be cross-checked periodically, to ensure they have not been affected by the laboratory environment with its frequent ramping up and down of strong magnetic fields. Demagnetization of samples can be achieved by subjecting them to an alternating field which is then smoothly reduced to zero, by reverse direct fields, or, especially in palaeomagnetic studies, by progressive heating of the sample. An alternating field demagnetizer can also be used to impart ARMs, by placing a current-carrying coil within the demagnetizing coil, to generate a small superimposed steady field ($\sim$0.08 mT).

This combination of the sensitivity of magnetic measurements of whole samples (remembering that the ferrimagnetic components occur most often in trace amounts) and the diversity of natural magnetic minerals, concentrations, grain sizes, compositions and morphologies enables rapid retrieval of magnetic records from soil and sediment sequences across the globe.

Quantitative estimation of the concentrations and/or contributions of individual magnetic components to the measured magnetic properties can be approached through a variety of means, usually assuming that the bulk

magnetization (M) is well represented by a linear addition of the magnetic constituents:

$$M = \sum M_i / x_i$$

where x_i is the proportion of the ith constituent. This simple additivity approach enables both mathematical mixing, i.e. the magnetic properties of the possible source constituents can be summed to find the magnetic properties of mixtures and 'unmixing', i.e. the magnetic properties of an environmental sample can be mathematically 'unmixed' in terms of its proportions of source constituents [22,23]. The unmixing can be achieved by multiple regression or optimization algorithms such as Simplex. To keep the models as simple as possible, constituents can be pre-selected, normally on the basis of independent mineralogical analysis of representative magnetic extracts from a selected subset of environmental samples. Conversely, magnetic data (such as remanence acquisition or demagnetization curves) can be unmixed with no *a priori* knowledge of possible constituents [24].

Because natural magnetic grains most often occur in trace amounts and in sub-micrometre grain sizes, independent mineralogical examination of such grains *in situ* is unfeasible for large numbers of samples. Where the magnetic grains are $\sim$ or >1 μm, optical and/or scanning electron microscopy of polished sections can be done. Where the grains are sub-micrometre in size, transmission electron microscopy (TEM) is needed. However, such techniques can only readily be applied to samples containing high concentrations of such small grains. The alternative approach is to remove as many of the magnetic grains as possible from the sample, in order to then analyse the grains by x ray diffraction, microscopy and elemental analysis (figure 14). Magnetic extraction procedures need to be carefully designed and implemented in order that they extract sufficient proportions of the magnetic carriers (i.e. the magnetic grains contributing to the magnetic properties of the whole sample) so as to be representative. Especially for natural samples containing SD and SP ferrimagnets, the key requirement for efficient magnetic extraction is the generation of high magnetic field gradients, within which such small grains can be trapped [25,26]. Before- and after-magnetic extraction, magnetic measurements should be performed, in order to identify the proportions of magnetic grains retrieved and hence the degree of representativeness of the extract. X-ray diffraction and microscopy of such extracts from a range of natural samples (deep-sea sediments, soils, suspended sediments in rivers) show that not only discrete magnetic grains are extracted in these procedures; significant amounts of quartz and other silicate grains nearly always appear, due to the presence of magnetic grains as inclusions within these diamagnetic or paramagnetic host particles (figure 15).

Recent advances in TEM techniques, using off-axis electron holography (e.g. [27]), enable direct visualization of magnetic grains and sub-grain structures at scales approaching the nanometre (figure 16(*a*) and (*b*)). An electron microscope produces a highly coherent beam of high-energy electrons, using an electron emitter in an

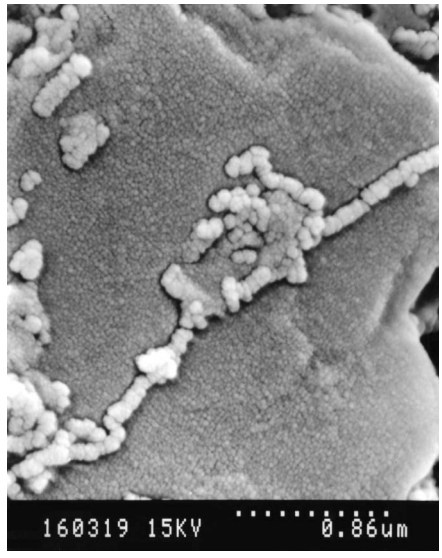

Figure 14. Scanning electron micrograph of chain of bacterial magnetites (photo by M. Hounslow from [7]). Copyright 1999. Reprinted with permission by Cambridge University Press.

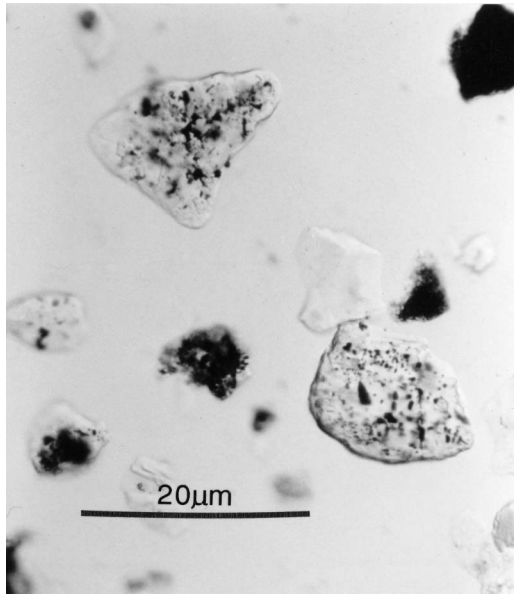

Figure 15. Optical micrograph showing magnetic particles occurring as inclusions within host diamagnetic quartz grains (photo by M. Hounslow from [7]). Copyright 1999. Reprinted with permission by Cambridge University Press.

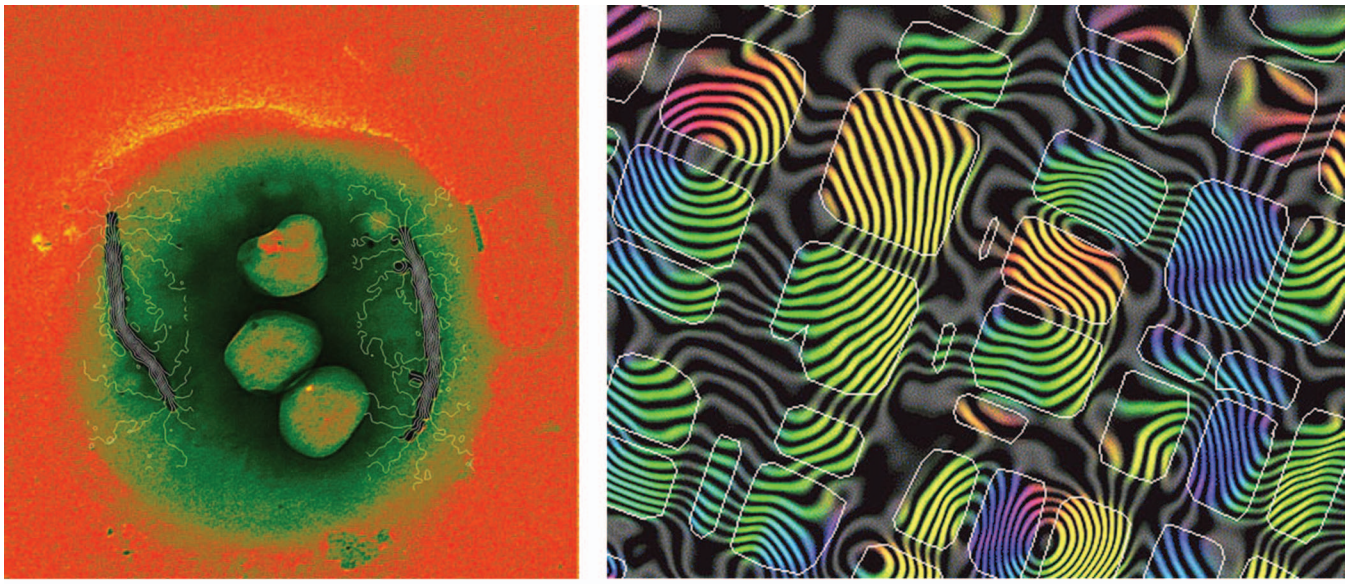

Figure 16. Off-axis holograms showing (*a*) magnetic field lines (the fine white lines) around the magnetic crystals made within a magnetotactic bacterium [28] and (*b*) small regions of magnetite, each about 100 nm in size (outlined in white), separated by regions of non-magnetic ulvospinel. The black lines show the magnetic field lines in the sample; the colours show the direction of the local magnetic field in each magnetite block [27].

'electron gun', and directs the beam onto a thin specimen using electromagnetic lenses. For electron holography, a positive charge is applied to an electron biprism (an ultrathin conductive fibre), positioned in an imaging lens perpendicular to the electron beam so that it splits the field of view. When a charge is applied to the biprism, overlap between the electron wave passing through the specimen and the reference (vacuum) wave is induced, creating an interference pattern, or hologram, in a slightly defocused image plane. These interference patterns change in position and contrast, depending upon the interaction between the magnetic moments of the specimen and the electron beam. In conventional electron microscopy, the objective lens creates a large vertical magnetic field ($\sim$2 T) at the plane of the sample. For holography of magnetic samples, the objective lens is switched off and a Lorentz lens, a minilens with a very low magnetic field at the object plane, is used to examine the specimen in close to field-free conditions. By then partially exciting the objective lens and tilting the sample, different in-plane magnetic field components can be applied to the specimen, enabling visualization of field lines, domain wall movements, hysteresis loops, and remanent states (figure 16).

These complementary analyses are more time-consuming than whole-sample magnetic measurements but enable structural, physical and elemental characterization of natural magnetic minerals, and, in turn, a more detailed understanding of sources of magnetic properties, minerals and their causal links with environmental change.

5. Magnetism and climate

The magnetic signatures of deep-sea sediments and of continental windblown dust (loess) deposits record precisely the imprint of global climate change during the last $\sim$2.5 million years. By applying our 'magnetic non-destructive evaluation' to samples from these sediment sequences, we can retrieve these climate records and use them to make quantitative estimates of past climate parameters, specifically, in the case of the Chinese Loess Plateau, of rainfall.

5.1 The Chinese Loess Plateau: 2.5 million years of changing monsoon intensity

Stretching from Xi'an in the south (where it provided the perfect construction materials for the populous Terracotta Army) to Beijing in the east, Tibet in the west and southern Mongolia to the north (figure 17), an enormous wedge of windblown loess—the Chinese Loess Plateau—spans an area of around 440×10^3 km^2. This loess wedge is thickest in the west, spanning more than 300 m vertical thickness near Lanzhou, and thinning to the east and south, to $\sim$150 m around Luochuan (figure 18) and Baoji. The loess consists of a mixture of mineral grains, including particles of quartz, feldspar, clay minerals such as chlorite and mica, minor amounts of haematite and goethite, and trace amounts of magnetite and titanomagnetite (variably oxidized to maghemite and titanomaghemite). The present

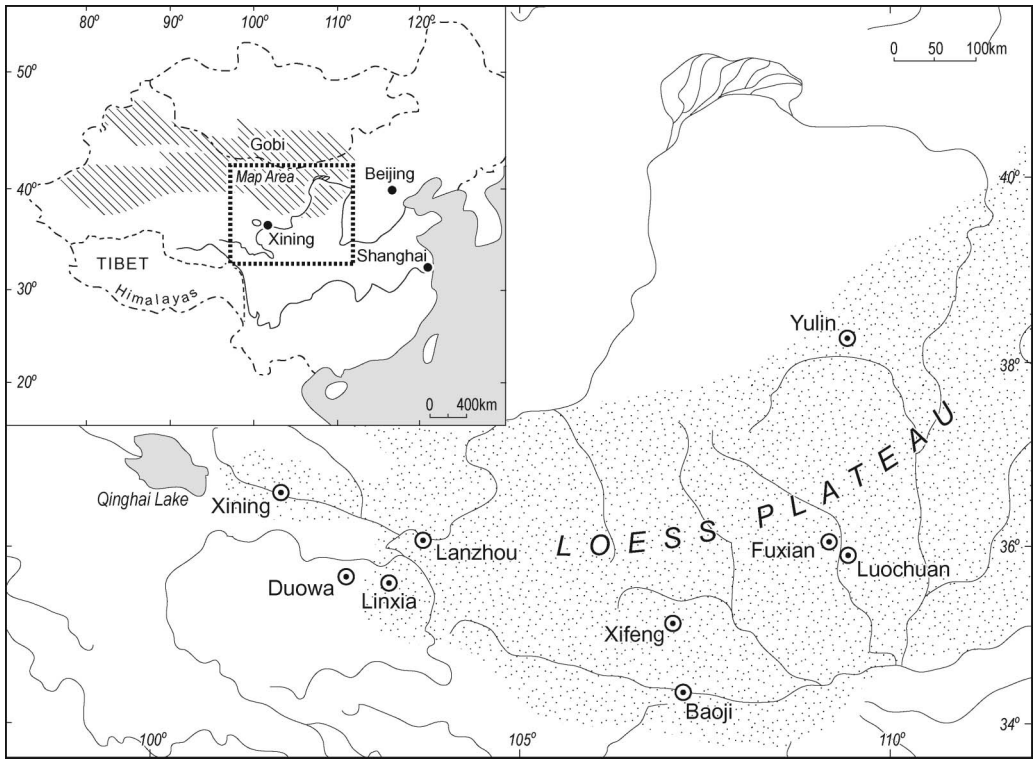

Figure 17. Location map for the Chinese Loess Plateau.

Figure 18. The interbedded windblown dust (loess, pale colour) and fossil soil layers (reddened) exposed in the sediment sequence at Luochuan, central Chinese Loess Plateau [12].

day climate of the Chinese Loess Plateau is dominated by the East Asian summer monsoon, which supplies up to 90% of the annual rainfall to the region, with southeasterly winds bringing moisture from the South Pacific. In winter, the winds blow in the opposite direction, from northwest to southeast, blowing dust from the desert areas of Mongolia. The rainfall that reaches the deep continental interior in the summer depends on the intensity of the summer monsoon (in turn determined by the amount of surface heating and the temperature of the southwest Pacific) but is much less than that delivered to the southern and eastern areas of the Plateau. Annual rainfall in the west of the Loess Plateau is $\sim$350 mm year^{-1}, increasing to $\sim$550 mm year^{-1} in the central Loess Plateau and $\sim$700 mm year^{-1} in the south.

In volume terms, the loess sediments ($\sim 2 \times 10^5$ km^3) are equivalent to, for example, the mountains of Scandinavia ($\sim 2.5 \times 10^5$ km^3). To generate such large volumes of dust, efficient breakdown of rocks in the dust source areas is needed, to produce those finer particles ($< \sim 63$ μm) capable of being picked up and transported by the wind. Such splitting of rocks can be achieved by the $\sim$9% volume expansion of water in daily freeze–thaw cycles (e.g. on the high Tibetan Plateau, a process likely to have been greatly enhanced during past glaciations) and/or by precipitation of salt crystals during evaporative conditions in deserts like the Gobi (figure 17). The particle size of the loess changes across the Loess Plateau, becoming finer towards the southeast, thus suggesting the deserts to the northwest as a key source (the traditional view). However, the magnetic content of modern desert samples is very low (susceptibility $\sim 5 \times 10^{-8}$ m^3 kg^{-1}) compared with the unmodified loess across the Plateau (susceptibility $\sim 20-30 \times 10^{-8}$ m^3 kg^{-1}). This suggests that the desert sands contain

insufficient detrital magnetic minerals (i.e. magnetic grains released from rocks by weathering and then available for transport by wind, water or ice) to be a key source for the loess. Also, the loess has variable but often extremely high loadings of beryllium-10, of between $0.5-5.5 \times 10^8$ atoms g^{-1}. Cosmic bombardment of the Earth's atmosphere is the major source of ^{10}Be ($T_{1/2} = 1.5$ Ma), from where it is then deposited at the Earth's surface in rain and snow. These high ^{10}Be loess values indicate that the dust was transported not from a desert source area but one exposed to $\sim$1 million years or more of moderate to high rainfall. Thick beds of glacial/periglacial silt occur on the Tibetan Plateau, to the west (figure 19), with magnetic susceptibility values of $\sim 25 \times 10^{-8}$ m^3 kg^{-1}. The cold, wet, tectonically-rising uplands of the Tibetan Plateau and the Himalayas are thus likely to have been the primary source for much of the Chinese loess, possibly via a 'dog-leg' transport path, first by winter wind transport to the NE to the Mongolian deserts, and then from there, by spring-time northwesterly winds, to the Loess Plateau.

Interbedded with the relatively unmodified layers of loess are layers which are reddened in colour (figure 18), and which display significantly higher magnetic susceptibility (up to $\sim 450 \times 10^{-8}$ m^3 kg^{-1}) than the loess layers ($\sim 20-30 \times 10^{-8}$ m^3 kg^{-1}). These layers contain slightly higher organic carbon content, some fossil pollen grains (albeit poorly preserved) and snail shells. They are buried soils (palaeosols), which formed at successive intervals at successive surfaces of the accreting Loess Plateau. The palaeosols formed during past climate stages when the climate was warmer and wetter than the colder and drier intervals when the loess was transported and deposited. More than 30 palaeosols occur in the long loess/soil sequences (figures 18 and 21—see section 5.2). They thus record more than 30 alternations in the strength of the winter (dry) and summer (wet) East Asian monsoon in the past. It is possible to both work out the age of these sediments, and calculate the changes in summer monsoon rainfall, from measurements of their magnetic properties.

Figure 19. Beds of silt- and finer-sized material, produced by splitting of rocks by freeze-thaw processes, Tibetan Plateau (photo by B. Maher from [12]). Copyright 1999. Reprinted with permission by Cambridge University Press.

5.2 Chronology and palaeoclimatology of the Chinese loess and palaeosol sequences

The magnetic properties of these sediments provide a record of palaeoclimatic information and also enable the sediment sequences to be dated. When the primary, detrital magnetic minerals in the loess (contributing the 'background' magnetic susceptibility of the least-weathered loess layers all over the Plateau) were dropped out of suspension by the wind and deposited on each successively accreted surface, they tended to align in the direction of the Earth's magnetic field at the time of their deposition. By taking sediment samples throughout the loess/soil sequences, orientated with respect to north and the vertical, their record of the magnetic declination and inclination of the geomagnetic field can be measured, for successive time intervals as each layer upon layer of loess was deposited. Because the Earth's geomagnetic polarity has reversed at known times in the past (figure 20 shows the geomagnetic

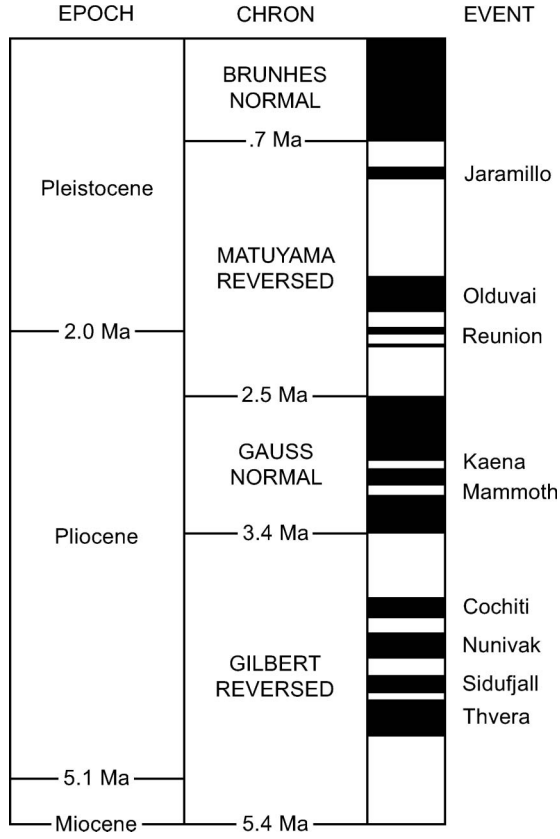

Figure 20. The geomagnetic polarity timescale (GPTS) for the last 5 million years.

polarity timescale, GPTS, for the last 5 million years), the loess sedimentary record of magnetic reversals can provide age control for the loess sequences. For the thickest loess/soil sequences, all six major geomagnetic polarity reversals of the last 2.5 million years are unambiguously recorded (figure 21), showing that loess deposition was initiated $\sim$2.5 million years before present (BP). This chronology can be refined in more detail by applying magnetic cyclostratigraphy to the loess/soil sequences (see below).

When these directional magnetic measurements were first made on the loess sequences [29], magnetic susceptibility measurements were also carried out. It became clear that the palaeosol layers had higher susceptibility values than the intervening, parent loess layers (figure 22). These changes in sediment type (loess to soil) and changes in magnetic susceptibility show strong correlation with the record of changes in the oxygen isotope composition of the deep-sea (figure 22). In glaciations, when large volumes of isotopically light oxygen (^{16}O) are 'locked up' in continental-sized ice sheets, the proportion of isotopically heavy oxygen (^{18}O) in the oceans increases. During interglacial stages, when the ice-sheets melt and release back into the oceans their previously stored ^{16}O, the proportion of ^{18}O in the ocean water decreases. Carbonate-forming marine plankton (foraminifera) take up oxygen from the ocean water with the 'same' $^{18}O/^{16}O$ isotopic ratio as the water (with a known amount of temperature-dependent fractionation). When they die, their carbonate shells become part of the sediment layers accumulating through time on the deep-sea floor. Deep-sea sediment cores can thus provide foraminiferal records of glacial climate stages (plankton recording relatively high $^{18}O/^{16}O$ isotopic ratio) and interglacial climate stages (relatively low $^{18}O/^{16}O$ isotopic ratio). The clear correlation between the loess/soil magnetic record and the deep-sea oxygen isotope record indicates that the monsoon in East Asia is linked with the expansion and contraction of the major ice sheets in the northern hemisphere. However, to quantify past changes in climate from the Chinese loess, we need to determine the magnetic composition of the sediments, which aspect of climate dominantly controls this magnetic signature, and what part of the magnetic record has been most sensitive to climate change.

In terms of magnetic susceptibility, the loess/palaeosol magnetic signal can be seen as a series of positive susceptibility shifts in the palaeosols, superimposed on a relatively constant background value in the loess ($\sim 20-30 \times 10^{-8}$ m^3 kg^{-1}). This can be most clearly demonstrated in the presently semi-arid western Loess Plateau sites, where the intervening, thick layers of loess have undergone very little weathering and show very little

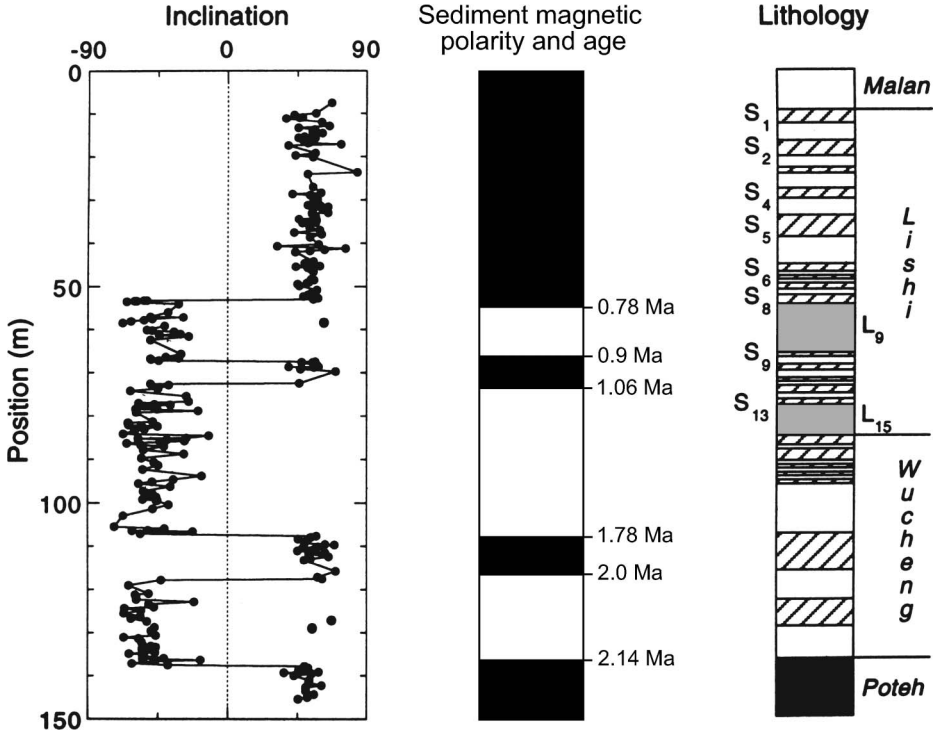

Figure 21. The stratigraphy (sediment layering) and magnetic inclination records for Luochuan, central Chinese Loess Plateau [29], and the geomagnetic polarity timescale. The switches in inclination values record each of the changes in the Earth's magnetic polarity over the last $\sim$2 million years (from [12]).

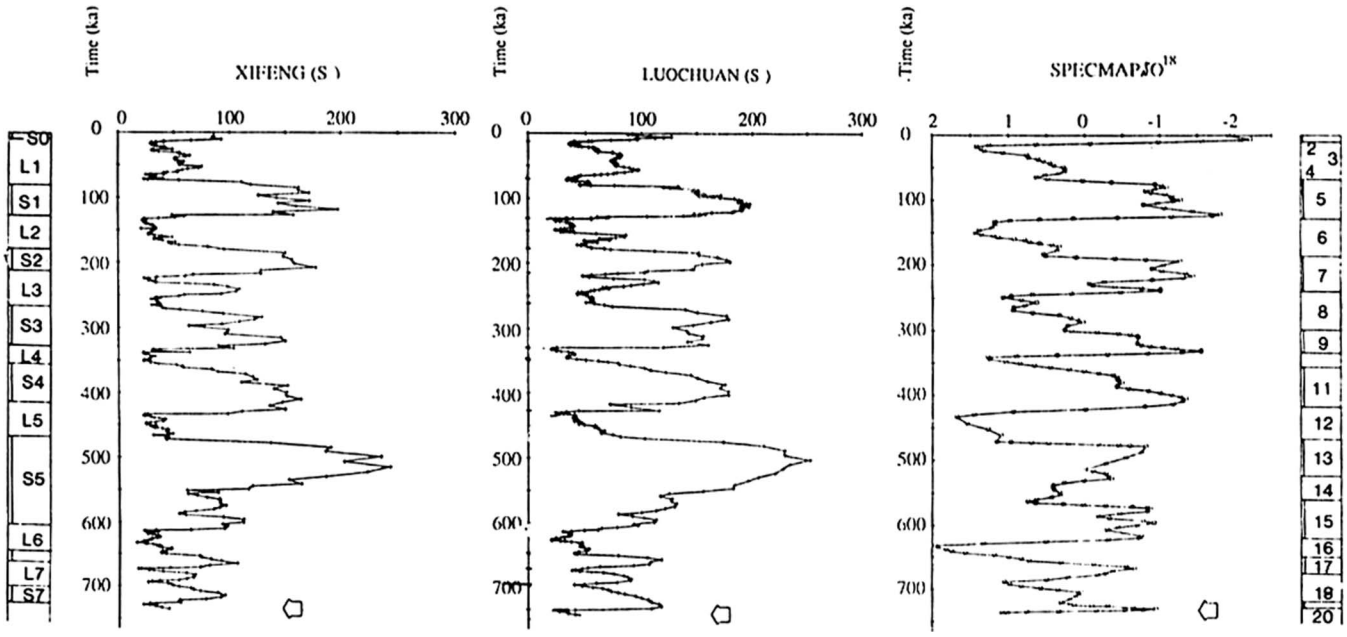

Figure 22. The stratigraphy and magnetic susceptibility records for two sites in the central Loess Plateau, Xifeng and Luochuan, and the deep-sea oxygen isotope record (from [29]).

magnetic change, whilst the soil layers show rapid susceptibility increases, up to values $\sim 120 \times 10^{-8}$ m^3 kg^{-1} (figure 23). Susceptibility thus clearly varies with time; it also, however, varies in space. Figure 23 shows the sediment stratigraphy and magnetic susceptibility data for three sites across the Loess Plateau, from west (Linxia) to central (Qinjiazhi) and south (Baoji), spanning the present day gradient in rainfall from semi-arid in the west to humid in the south. The last glacial loess layer (L_1) typically has susceptibility values of 30×10^{-8} m^3 kg^{-1} in the arid western areas, 60×10^{-8} m^3 kg^{-1} at the central Plateau and 160×10^{-8} m^3 kg^{-1} for the most humid southern area. For the present interglacial and last interglacial soils ($Soil_0$ and $Soil_1$), susceptibility values along this west–central–south transect increase markedly towards the more humid area. In terms of the concentration of magnetic minerals, the mean susceptibility values at the central Loess Plateau of 63×10^{-8} m^3 kg^{-1} for the loess and 145×10^{-8} m^3 kg^{-1} for the soils indicate a magnetite content of $\sim 0.1\%$ and 0.26%, respectively. When the magnetic properties of the soil and loess samples are measured on separated particle size fractions (i.e. sands, >63 μm; silts, 2–63 μm, and clay, <2 μm), the clay-sized fractions of the soils are found to be six times more magnetic than the sand fractions, making the greatest contribution by far to whole-sample saturation remanence, susceptibility, frequency dependent susceptibility, ARM and low-field remanence [7,30]. For the loess samples, the peak magnetic contributions arise in the coarse silt fraction (~ 30–50 μm).

Thermomagnetic experiments (figure 24) show that the magnetizations of the loess and soils are dominated by magnetite, with its Curie point of ~ 580°C, and some maghemite. The inflections in the heating curves at ~ 400°C reflect the oxidation of strongly magnetic maghemite to weakly magnetic haematite, resulting in the loss of remanence seen in the cooling curves. The amount of maghemite appears to vary across the Loess Plateau. For the palaeosol at Luochaun, in the central Loess Plateau, the remanence loss upon cooling is $\sim 40\%$; for the arid, western site, the loss is $\sim 70\%$. Measurements of room temperature remanence acquisition (figure 25) for the uppermost palaeosol (S_0), first loess layer (L_1) and last interglacial soil layer (S_1) from west (Linxia) to central (Qinjiazhi) and south (Baoji), show distinct inflections at 0.1 T, pointing to the presence of both ferrites (magnetite/maghemite) and imperfect antiferromagnets (haematite/goethite) in the parent loess and the palaeosols. The haematite/goethite component, evident in applied fields beyond ~ 0.2 T, accounts for only $\sim 6\%$ of the saturation remanence in the loess layers and even less, $\sim 2.5\%$, in the soils. Remembering, however, the much weaker magnetic properties of haematite, this means it is typically ten times more abundant than the ferrimagnets in these sediments. Also, to produce the visible pigmentation and reddening of the palaeosols compared with the 'buff-coloured' parent loess (figure 18), some of the haematite in the soils must be extremely fine-grained (<25 nm; [19]) and formed *in situ*, during soil formation, rather than 'inherited' from the loess. Hysteresis loops for the palaeosols are always steeper

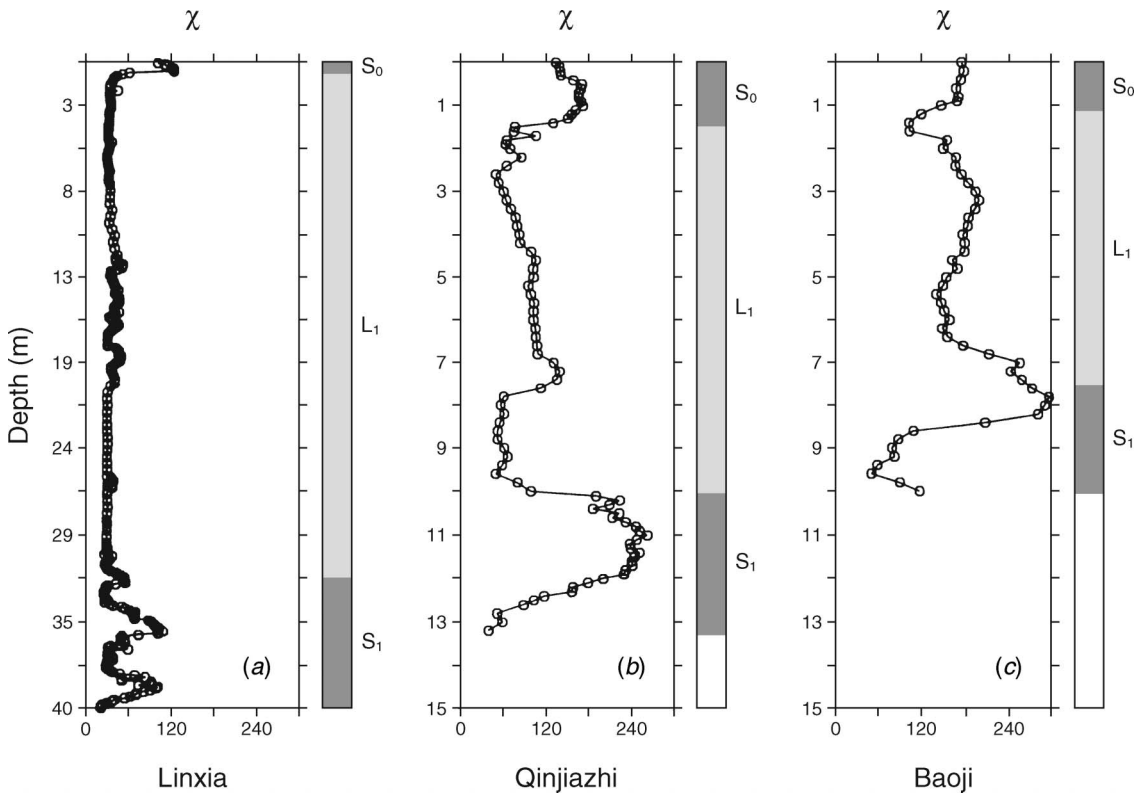

Figure 23. Stratigraphy and magnetic susceptibility records for three sites spanning the Chinese Loess Plateau from (*a*) the arid western region, Linxia; (*b*) the central, more humid area, Qinjiazhi; (*c*) the most humid south, Baoji. The western site has the thickest loess/soil sequence (highest sedimentation rate) and the least-developed magnetic enhancement in the palaeosols. The wetter sites to the east and south have thinner sequences and more developed soil magnetic enhancement.

and narrower than those from the loess. For the west–central–south transect, coercive force values vary between 9 and 11 mT for the loess and 7.7–8.5 mT for the soils.

Further distinct differences in magnetic properties between the loess and the soils reflect differences in the magnetic grain size of their ferrimagnets. The palaeosols display significant frequency dependence of their magnetic susceptibility (measured at 0.47 and 4.7 kHz), indicating the presence of ferromagnetic grains at/around the superparamagnetic size threshold ($\sim$0.03 μm at room temperature). Shifting to higher measurement frequency causes such grains to 'block in' and behave as single domain rather than superparamagnetic, resulting in lower χ ($\sim$10–15% lower in the palaeosols here). The palaeosols also show higher anhysteretic remanence values (most evident when normalized with the saturation remanence, to remove the effect of changes in magnetic concentration), indicative of ferrites with grain sizes $\sim$0.03 μm. These granulometric data suggest that the major cause of the higher susceptibility values of the palaeosols is increased concentrations of ultrafine ($<\sim$0.05 μm), single domain and superparamagnetic magnetite and maghemite [31,32]. Figure 26 shows a magnetic biplot combining frequency dependent susceptibility data with χ_{ARM}/SIRM ratios for the loess and soils, and, for comparison, for sized, synthetic, submicrometre magnetites (dispersed in a non-magnetic matrix) and coarser-grained, crushed natural magnetites. The least-weathered loesses (e.g. $L1_1$ and $L1_2$) plot towards the pseudo-single domain and multidomain magnetites of $>\sim$5 μm diameter; the most-developed soils plot towards the superparamagnetic/single domain size range ($<$0.03 μm). These grain size contrasts are confirmed through low temperature susceptibility measurements (figure 27). Upon warming from liquid nitrogen temperature, a loess sample from the western site (Linxia) shows a major change in its susceptibility at $\sim$125 K (i.e. at the Verwey transition, reflecting a structure phase transition from cubic to distorted-cubic spinel), most typical of multidomain magnetic behaviour. Beyond this point, there is a slight decrease in susceptibility with increased temperature, indicative of a minor paramagnetic component. The Linxia soil sample, in contrast, shows a rapid and then slower rise in susceptibility upon warming, behaviour characteristic of superparamagnetic ferrites 'unblocking' as their degree of thermal disordering increases. Using both frequency dependent and temperature-dependent

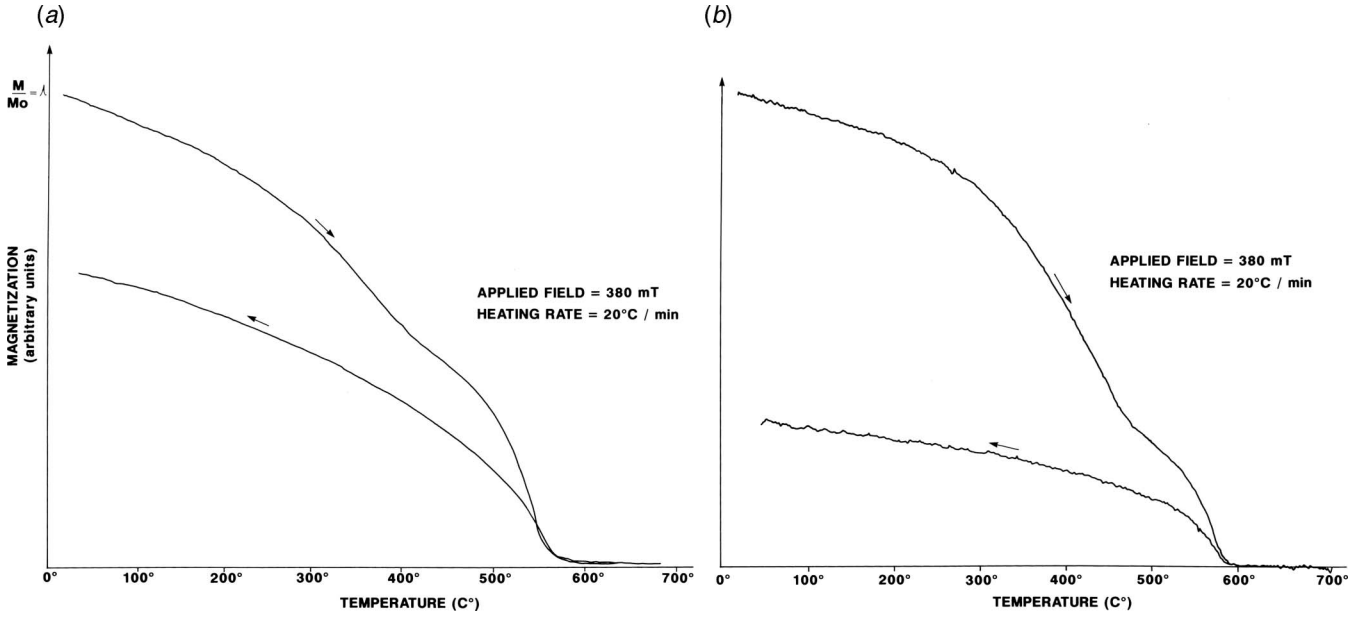

Figure 24. Thermomagnetic analysis for (*a*) a strongly developed palaeosol (S_5) from Luochuan (susceptibility $= 256 \times 10^{-8}$ m^3 kg^{-1}) and (*b*) palaeosol S_0 from the arid western site, Linxia (susceptibility $= 110 \times 10^{-8}$ m^3 kg^{-1}) (from [12]). Magnetization falls at the Curie point for magnetite ($\sim 580^{\circ}$C), but there is also a slight decrease in magnetization at $\sim 400^{\circ}$C, reflecting the oxidation of maghemite to haematite. Because of this conversion of a strongly magnetic ferrimagnet to a weakly magnetic canted antiferromagnet, the magnetization of the sample as it is cooled is significantly less than its original magnetization.

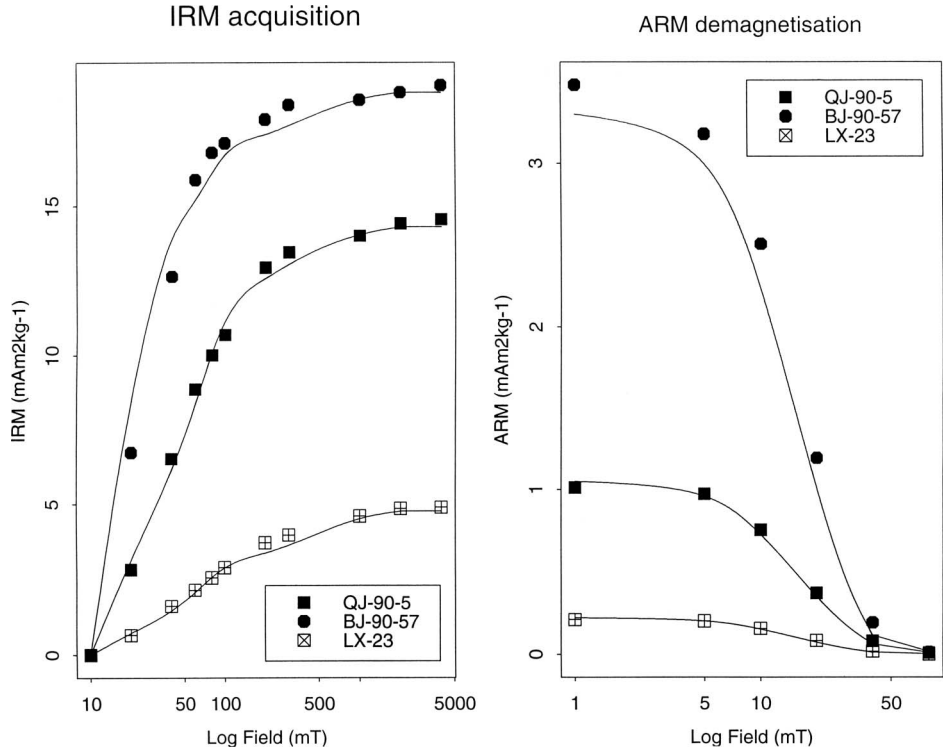

Figure 25. Room temperature magnetic remanence acquisition and ARM demagnetization curves: loess L_1 from Linxia (LX-23), palaeosol S_0 from Qinjiazhi, near Luochuan (QJ-90-5), and palaeosol S_1 from Baoji (BJ-90-57) (from [12]). Compared with the wetter central and southern sites, the semi-arid western site shows least remanence acquisition, especially at low applied fields.

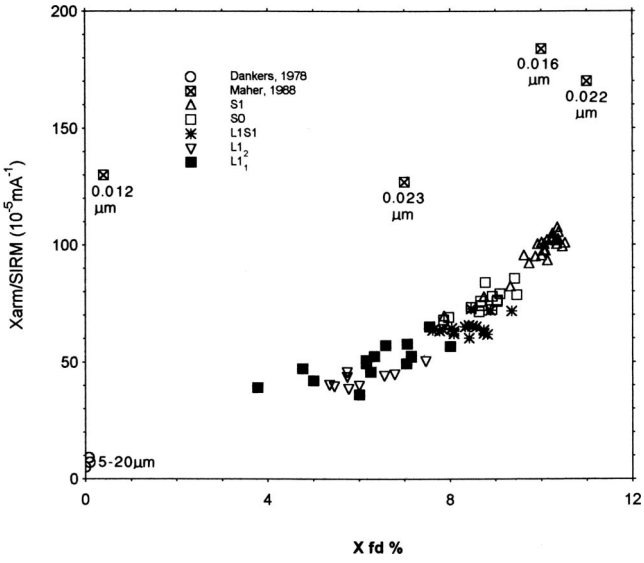

Figure 26. Frequency dependent susceptibility (expressed as a % of the low frequency susceptibility) versus the ratio of ARM (normalized for the dc field) and saturation remanence for loess and soil samples from Qinjiazhi, near Luochuan, and for some sized, pure magnetites (from [12]). The least-weathered loess samples trend towards the multidomain-sized magnetites, whilst the increasingly developed soils move towards the superparamagnetic/single domain magnetite powders.

susceptibility measurements, and drawing on Néel's theory, it is possible to estimate the magnetite grain size distribution (normalized) in the palaeosols (figure 28, [33]).

Using the low temperature and room temperature remanence and susceptibility data, the magnetic mineralogy of the Chinese loess and palaeosols can be quantitatively unmixed in terms of specific magnetic minerals and magnetic grain sizes/domain states. For a central Loess Plateau site, this mathematical unmixing shows that the 'background', rather constant magnetic properties of the unweathered loess are dominantly contributed by MD magnetite and maghemite grains (0.2‰), with additional but minor magnetic contributions from haematite (6–9‰) and paramagnetic silicate minerals (e.g. iron-rich clays). In contrast, the magnetic properties of the palaeosols reflect the presence of an additional admixture of superparamagnetic (~0.3‰) and single domain (~0.9‰) ferrimagnets, and a slightly reduced contribution by haematite (4–8‰).

5.3 Mineralogy, morphology and source of the loess/palaeosol magnetic minerals

To identify the nature of the climate–magnetism connection, the origins of the loess and palaeosol magnetic minerals need to be identified. Additional information on

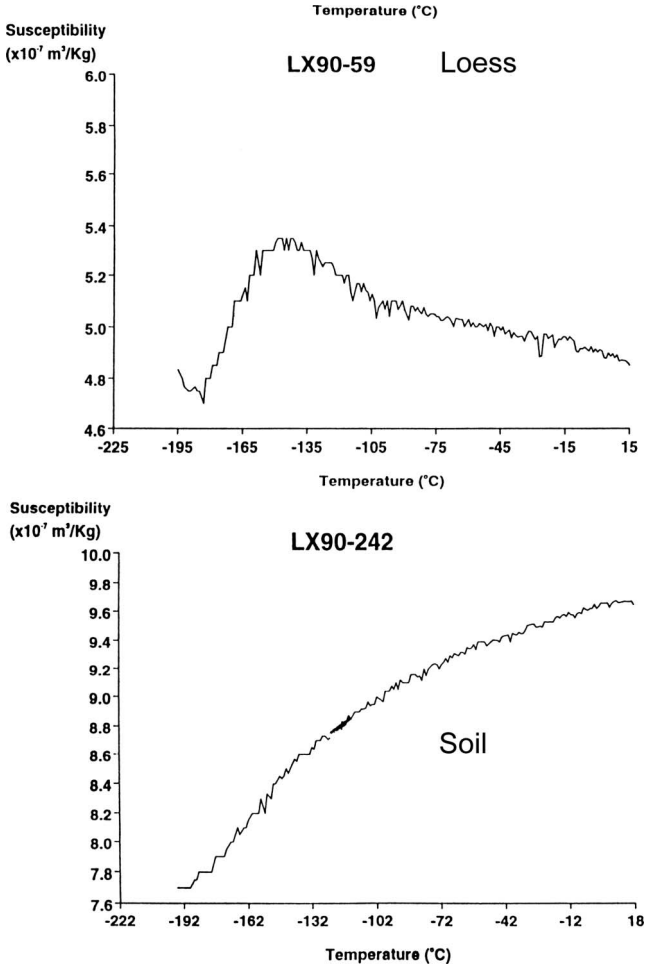

Figure 27. Low temperature measurements of susceptibility for samples from the arid western site, Linxia: (top) loess L_1 (LX-90-59) and (bottom) palaeosol S_1 (LX-90-242) (from [12]).

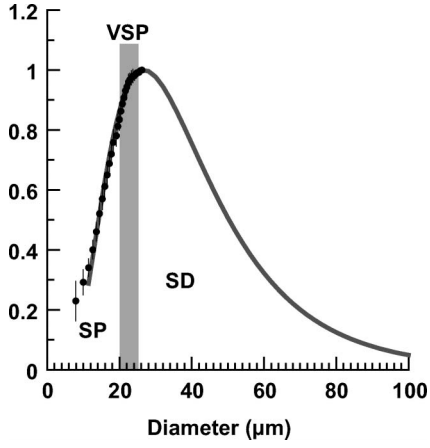

Figure 28. Grain size distribution for the superparamagnetic/single domain ferrimagnet fraction of the palaeosols, calculated from low temperature and frequency dependent susceptibility measurements (from [33]).

Figure 29. Scanning electron micrograph of detrital, rock-derived magnetite and titanomagnetite crystals from the loess (photo by Maher, 1999). Copyright 1999. Reprinted with permission by Cambridge University Press.

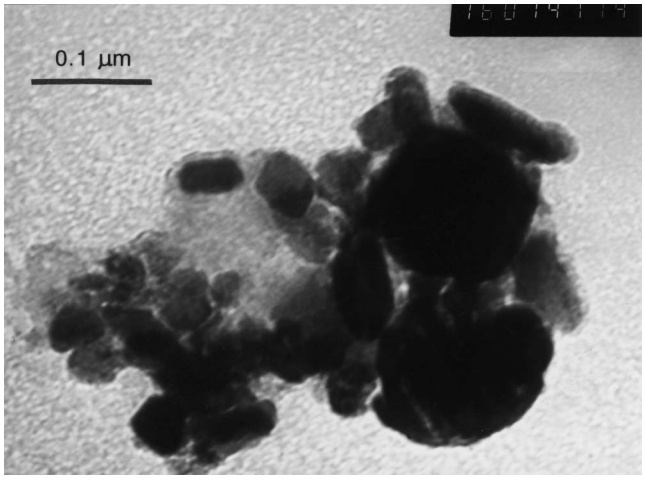

Figure 30. Transmission electron micrograph of the sub-micrometre, pure magnetites/maghemites from the palaeosols [8].

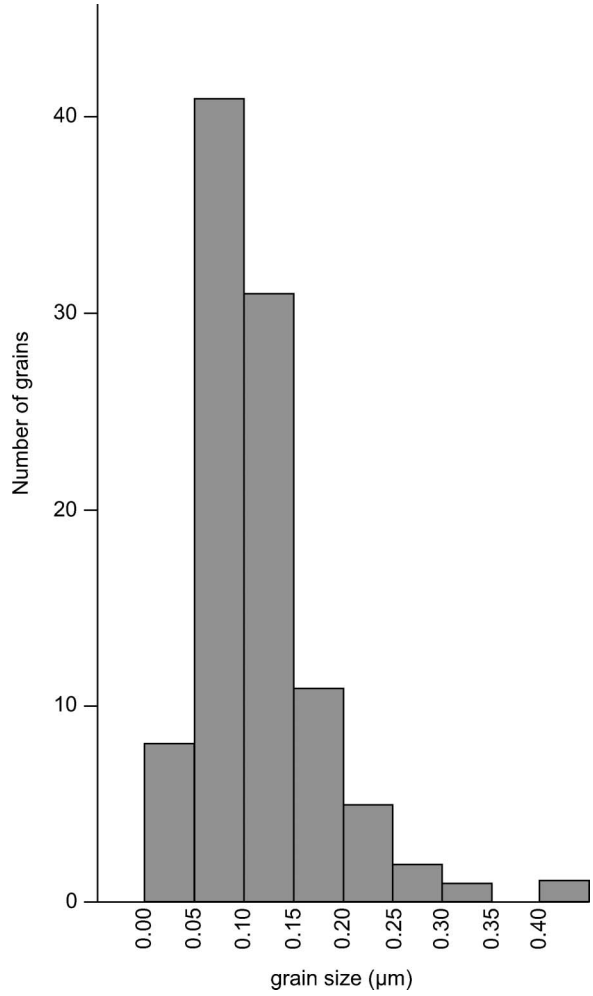

Figure 31. Grain size distribution from grain measurements of electron micrographs, magnetic extract, Luochuan palaeosol (from [8]).

how they formed can be gained from direct examination of the size and shape of the magnetic grains by microscopy, and of their composition by X-ray diffraction and elemental analysis. Because they occur in these sediments in trace amounts, they first need to be extracted magnetically, from a representative subset of samples. Magnetic extraction efficiencies for the loess and palaeosol samples range from 40–50% of the susceptibility-carrying minerals, 80–85% of the ARM carriers, and 70–80% of the saturation remanence carriers. Analysis of the extracted grains identifies two distinct populations of ferrimagnets; one group consists of 'large' magnetite/maghemite grains ($> \sim 1\ \mu$m), the other of ultrafine grains, $\sim 1-400$ nm. Figures 29 and 30 show typical examples of the two distinct grain types. The 'large' grains (figure 29) comprise a mixture of intact and chipped geometric crystals, of variable composition (some containing titanium, others titanium-free). These crystals are of igneous origin, and have been released from source rocks by weathering and erosion. These lithogenic grains comprise the 'background' ferrimagnetic population of the loess, and have been blown by the wind to be deposited within the unweathered loess. In contrast, the ultrafine, sub-micrometre ferrimagnets (figure 30) that additionally occur within the palaeosols are composed solely of iron and oxygen. Whilst they are very variable in size, they are generally well crystalline, often showing

clear cubic or hexagonal outlines. Clustering of (superparamagnetic-sized) crystallites around larger grains is evident. The size, composition and morphology of this ultrafine ferrimagnet population is very similar to magnetic grains formed *in situ* in modern soils (figure 7). They also closely resemble magnetites produced synthetically in laboratory conditions, through controlled rates of oxidation of ferrous iron suspensions [10]. In soils, Fe^{2+} can be produced (even in generally oxidizing soils) through the action of Fe-reducing bacteria, which 'switch on' during periods of soil wetness and in soil micro-zones, where oxygen levels are low. Under these conditions, they decompose organic matter using Fe^{3+}-oxides as their terminal electron acceptor [34]. The Fe^{2+} that results is released into the soil matrix where, upon partial oxidation, the Fe^{2+}/Fe^{3+} mix that is required for the formation of the inverse spinel structure and composition of magnetite is achieved. The whole-sample magnetic measurements and electron microscopy of the magnetic extracts are in general agreement in identifying that the grain size distribution of the soil-formed (pedogenic) magnetite is rather constant (figure 31; superparamagnetic grains are less well extracted magnetically than larger grains and so tend to be under-represented in the electron microscopy). The laboratory experiments on magnetite formation show that the grain size distribution of precipitated magnetites changes under differing conditions of pH, temperature, oxidation rate, and Fe concentration

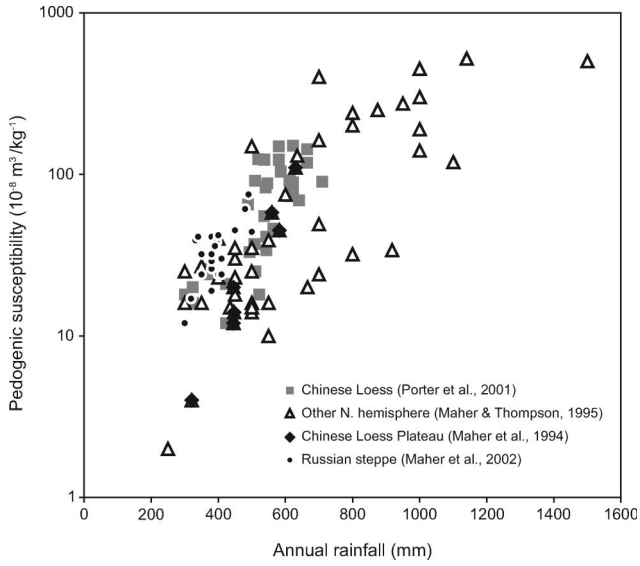

Figure 32. Pedogenic susceptibility versus annual rainfall for the modern soils across the Chinese Loess Plateau and across the Russian steppe (from [35]).

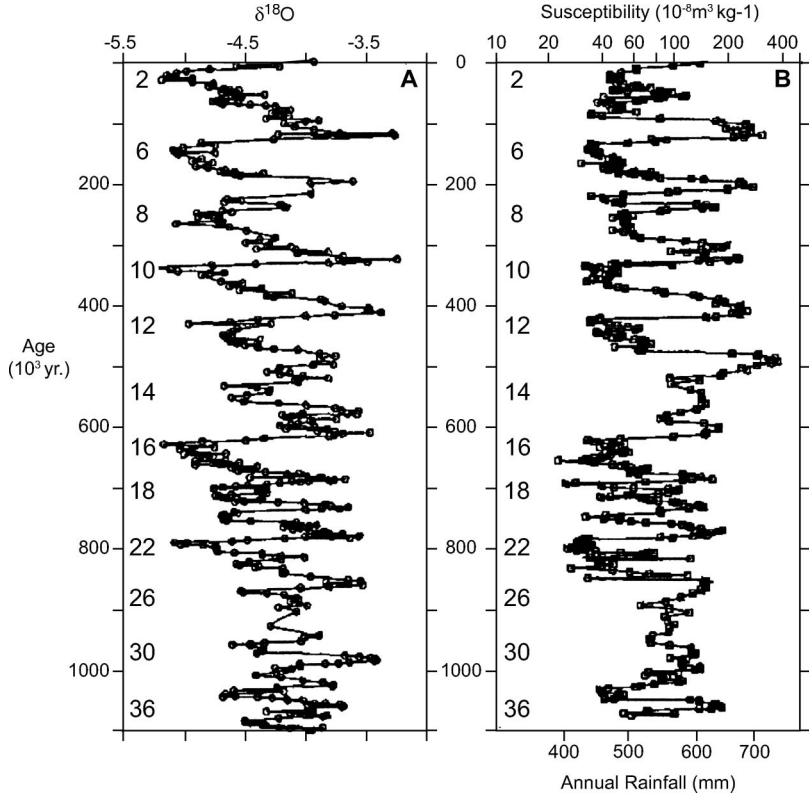

Figure 33. Magnetic susceptibility values, and the rainfall values calculated from the soil magnetism/rainfall transfer function, for the central Loess Plateau for the last 1 million years (from [36]).

[10]. The observed constancy of magnetite grain size in the Chinese palaeosols is likely to reflect magnetite precipitation under a specific set of soil micro-environmental conditions which favour the activity of the Fe-reducing bacteria. (For instance, the laboratory conditions which produce the magnetite grain size distribution observed naturally in the palaeosols comprise pH at $\sim$7.5 and an oxidation rate of 4 ml air/minute.)

A link between Fe^{2+} formation by bacteria in temporarily wet conditions and subsequent precipitation of ultrafine-grained, Fe^{2+}/Fe^{3+}-bearing magnetite upon soil drying suggests the basis of the observed magnetism/climate link: soils subjected to more rainfall are likely to contain more, ultrafine (superparamagnetic/single domain) magnetite. This hypothesis will hold until soils are too frequently or permanently wet; under these conditions, Fe oxides are either lost from the soil by excess acidity or permanently reduced (rather than partially oxidized, as required for magnetite formation). Conversely, in the case of the presence of too little water, as in arid soils, formation of Fe^{2+} is precluded. Formation of the more oxidized iron compounds, haematite and goethite, is favoured instead. This rain/magnetism hypothesis can be tested by measuring the magnetic properties of modern soils across modern rainfall gradients, including the modern soils of the Chinese Loess Plateau and, for an independent test, the modern soils across the loess-mantled Russian steppe from the Caucasus to the Caspian Sea (figure 32). For these modern soils, their *in situ* pedogenic magnetic susceptibility (i.e. the maximum soil susceptibility minus the parent loess susceptibility) is found to increase with increasing levels of annual rainfall to a peak at $\sim$1500 mm rain/year, and

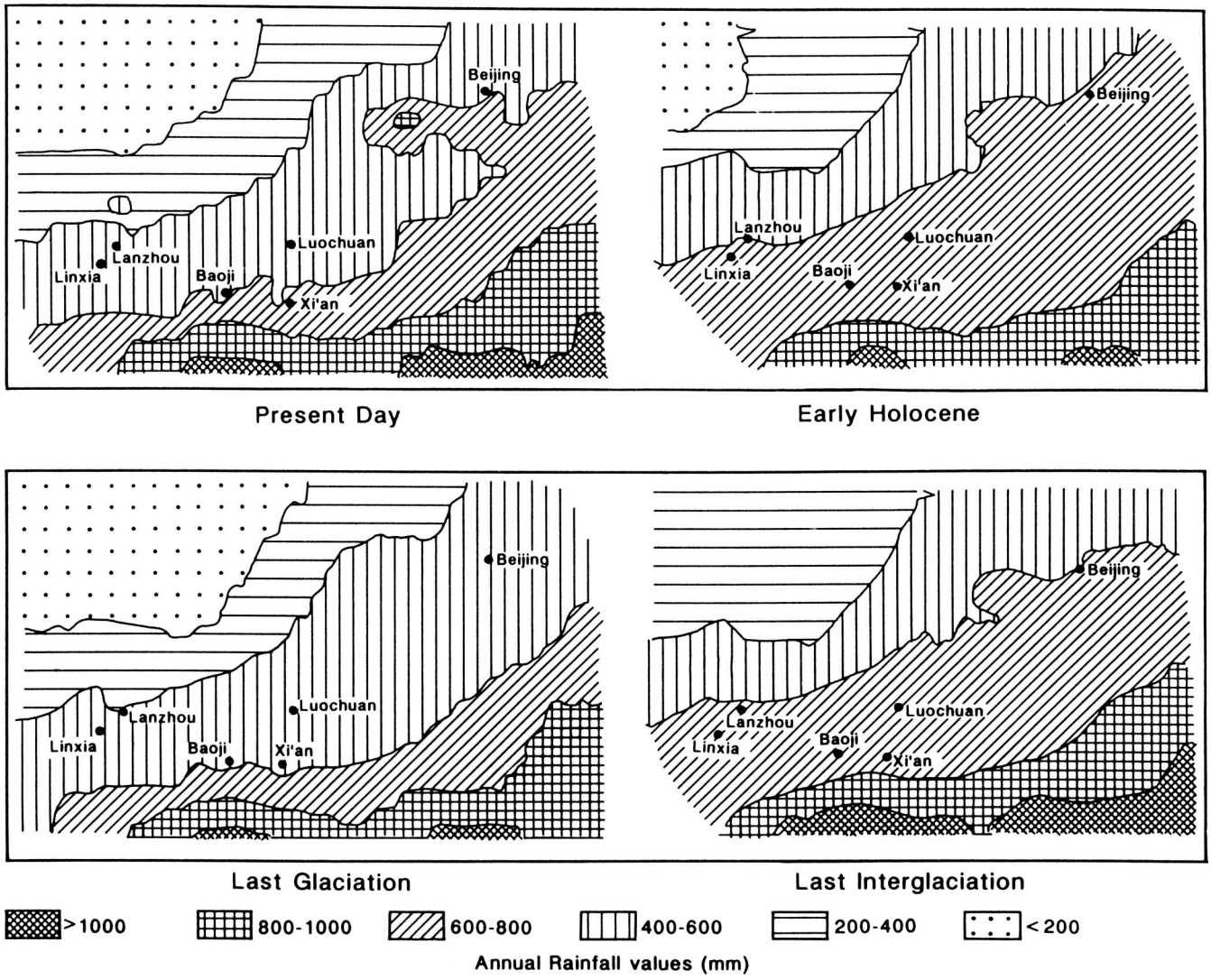

Figure 34. Spatial variations in annual rainfall across the Chinese Loess Plateau, early Holocene (i.e. the present interglacial), last glacial maximum ($\sim$20,000 years BP) and the last interglacial ($\sim$125,000 years BP) from [37].

then decreases at higher rainfall totals ($\sim$3000 mm yr^{-1}). A magnetism/rainfall transfer function (derived from least-squares regression analysis) can be calculated from this modern day relationship. This 'climofunction' can then be applied to the $\sim$33 successively buried palaeosols throughout the Chinese loess/palaeosol sequences, in order to estimate palaeo-rainfall for each soil-forming period through the last $\sim$2.5 million years (figure 33).

These palaeo-rainfall estimates show how the East Asian summer monsoon has varied in intensity through time and space. Higher rainfall than at present is identified at past intervals in our present interglacial stage (figure 34), with +25 to +80% more rain for the presently semi-arid western Loess Plateau area, and +5 to +25% for the more humid south and east. For the last glacial stage ($\sim$20,000 years ago), rainfall was reduced by up to $-$50%, with greatest desiccation in the presently humid southern area. For the previous interglacial stage ($\sim$125,000 years ago), summer monsoon intensity was again increased, by between +23 to +41%.

These rainfall records are significant because they provide long time series upon which frequency analysis can be carried out to identify the cyclicity of the past climate changes (see below). They also enable testing of general circulation models (GCMs), by providing long time series of climate data against which the model data can be compared. For example, GCMs run for the last interglacial interval postdict similar magnitudes of rainfall increase but locate the zone of enhanced rainfall too far to the east. Similarly, for our present interglacial, the GCMs postdict increased monsoonal rainfall at 5–6000 years BP for this region but at this time, the East Asian summer monsoon had decreased in intensity (figure 35). The models then indicate diminished monsoon intensity from $\sim$5000 years BP onwards, again not the case from our palaeo-data record. Improvements to the GCMs can be sought, whether in terms of enhanced spatial resolution or more realistic handling of key input data, such as changes in sea surface temperature, which may play a particularly significant role in subduing the East Asian summer monsoon at the mid-Holocene [38].

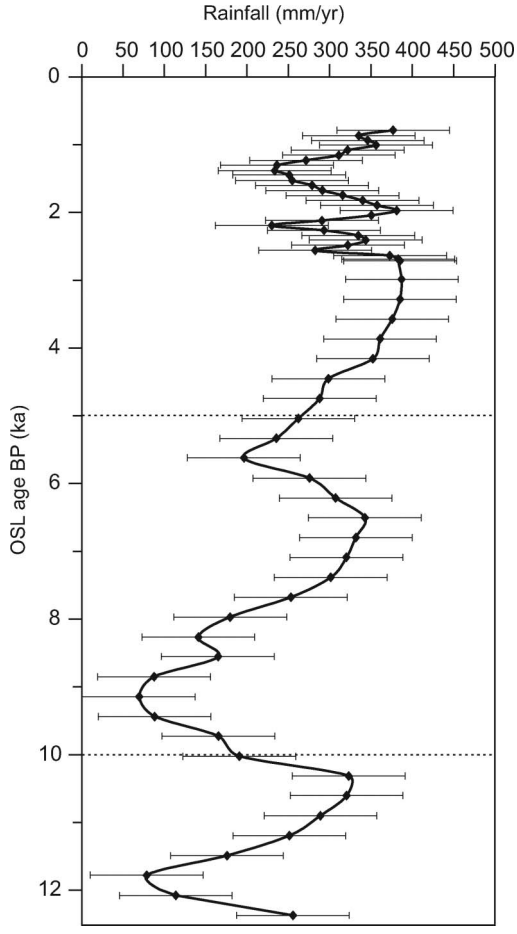

Figure 35. High-resolution Holocene rainfall record for a western Loess Plateau site (Duowa) (from [39]).

6. Orbital forcing of climate and magnetic cyclostratigraphy

The demonstrated coherence between the record of changes in the loess/palaeosol magnetic properties and the deep-sea oxygen isotope record (figure 22) reflects the response of both to orbitally-forced variations in climate. Changes in the Earth's orbit and axis of rotation are periodic and can be accurately calculated. They are caused by gravitational interactions of the Earth with the Sun, the Moon and the other planets, and give rise to cyclic changes (figure 36) in the eccentricity of the Earth's orbit (with main periods of $\sim$100,000 and 400,000 years), the Earth's axial tilt (varying between 22° and 24.6°, with a period of $\sim$41,000 years) and its axial precession (the movement of the rotation axis around a circular path, with a period of $\sim$19,000–23,000 years). These cyclical variations in the Earth's orbit affect the global, latitudinal and seasonal distribution of the solar radiation received at the Earth's surface, and thus fundamentally drive changes in the Earth's climate system. This concept of orbital forcing was first envisioned by Croll [40] and then quantified by Milankovitch [41]. Frequency analysis of long climate records had to wait until 1976, when two deep-sea sediment cores from the South Pacific were analysed for three climatic indices, including the foraminiferal oxygen isotope record [42]. These data indicated that the cores contained records of the last 9 glacial and intervening interglacial stages (spanning the past $\sim$450,000 years). The climatic variance of all the records was found to be concentrated in three discrete spectral peaks, at periods of 23,000, 42,000, and approximately 100,000 years (containing, respectively, about 10%, 25%, and 50% of the climatic variance). This dominance of the 100,000 year orbital forcing in driving glacial and

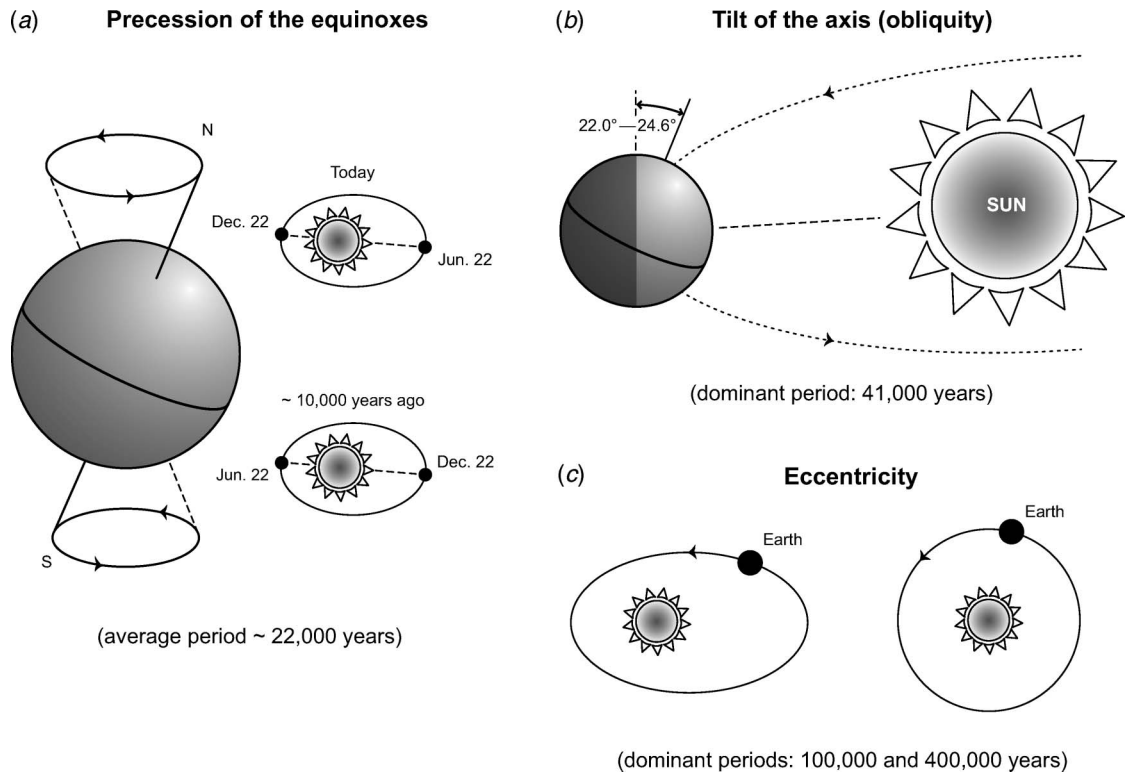

Figure 36. Earth's orbital variations (from [39]).

interglacial cycles is difficult to explain, given that changes in eccentricity result in very small changes in the total solar radiation received—at most 0.2% [43]. Amplifiers within the Earth's climate system must induce significant signal gain in this orbital forcing mechanism. The other orbital variations result in changes in the seasonal distribution of solar radiation. The tilt, or obliquity, of the Earth's axis is responsible for the seasons; an increase in tilt angle causes increased seasonal contrasts in both hemispheres, through an increase in local summer insolation and a decrease in local winter insolation. This seasonal contrast effect is felt most markedly at high latitudes. The influence of precession is also dependent on the eccentricity cycle. Currently, precession is close to its maximum, so that the Earth is at aphelion on 22 June, resulting in slightly cooler summers in the northern hemisphere and colder winters in the southern hemisphere. On 22 December, the Earth is nearly at perihelion, inducing milder winters in the northern hemisphere and hotter summers in the southern hemisphere. Precession will result in the northern hemisphere summer solstice occurring at perihelion in $\sim$11,000 years from now, when the seasonal contrast between the hemispheres will be the opposite of the present day.

Because these orbital cycles are recorded in the sedimentary record—whether by changes in sediment type, geochemistry, fossil assemblages, geochemistry and/or magnetic properties—and because astronomers can compute the past variations in eccentricity, obliquity and precession (e.g. [44]), astronomical and individual 'target' curves can be computed, for example, of summer insolation at any given latitude at any season (e.g. [45,46]). The sedimentary, climate-responsive properties, for example, foraminiferal oxygen isotope record [47] or the magnetic susceptibility record of the Chinese loess and palaeosols, can then be dated by comparison with the astronomical target curves. These astronomically-derived chronologies, independent of radiometric dating, have been used to refine the geomagnetic polarity timescale (GPTS). The GPTS was originally constructed using the seafloor magnetic anomaly patterns, dated by interpolation between potassium/argon-dated calibration points. A new astronomical polarity timescale (APTS) was constructed from 2 million year-long Quaternary marine sediment sequences in the Mediterranean Sea, which contained records of magnetic reversals, and successive organic-rich sediment layers tied to maxima in the summer insolation target curve. The new APTS indicated age discrepancies of 5–10% with the GPTS; the APTS ages for the reversals being consistently older. The APTS has since been substantiated by results from a new 40Ar/39Ar (single crystal) laser fusion dating technique [49,50].

Attempts to derive an orbitally-tuned timescale for the magnetic properties of the Chinese loess/palaeosol sequences identify good agreement between the loess/soil

magnetic susceptibility and the deep-sea oxygen isotope record, especially over the last 1.5 million years [36,50]. The influence of the eccentricity and obliquity components of orbital forcing are clear; the build-up and melting of northern hemisphere ice sheets (the dominant component reflected by the deep-sea oxygen isotope record) and Asian loess deposition and subsequent weathering to form soils are linked by common forcing factors. However, problems remain in fine-tuning of the two records. In particular, the positions of the magnetic reversals within the loess/soil sequences vary due to magnetic 'overprinting' by the effects of subsequent soil formation, and the precessional signal is poorly recognized. For the last $\sim$12,000 years (figure 35), the higher resolution magnetic loess/soil record reveals alternating and abrupt phases of humidity and desiccation at sub-Milankovitch frequencies throughout the present interglacial, Holocene period. Such millennial and sub-millennial cyclicities, which appear almost ubiquitous in Holocene sequences across both hemispheres, are thought to be linked with solar forcing and changes in ocean circulation (e.g. [51,52]). Some studies have attempted to link changes in the last glacial East Asian monsoon record with very large iceberg-discharge events in the North Atlantic Ocean (e.g. [53]) but the age control for both sets of records may be insufficient to substantiate these proposed links at this stage.

7. Conclusions

Magnetism has previously played a key role in geophysics and the Earth sciences in the past, one outstanding example being magnetostratigraphy and its breakthrough contribution to development of a new field, plate tectonics [54]. Environmental magnetism, using the record of variations in the magnetic properties of sediments, has become the latest magnetic development in geophysics, making a major and growing impact on our understanding of past and present climate and environmental changes on our planet. These environmental magnetic records encompass natural archives of past rainfall, as discussed here for the Asian loess/palaeosol sequences spanning the last $\sim$2.5 million years, but also for other regions including the Mediterranean, and the loessic areas of North America. Further, underlying the loess/palaeosol sequences of China are additional terrestrial sediment layers, the so-called 'Red Clay', which may record palaeo-rainfall over the last $\sim$20 million years. Other types of environmental magnetic archives record other changes across the global scale, including iceberg rafting in the North Atlantic [55] and the Southern Ocean, the timing and effects of increased dust transport from Africa, human impacts on rates of lake sedimentation, identification of natural biomagnets in a range of organisms (birds, fish, insects, humans) and mapping and measuring of particle pollution sources. A current development in environmental magnetic studies of climate change involves use of magnetic measurements to identify the source, iron mineralogy, grain size and rate of flux of windblown dust into the oceans. Windblown dust containing iron-bearing grains can have significant impact on climate, both in terms of changing the radiative properties of the atmosphere and changing the biogeochemistry of the oceans, and changing the carbon dioxide contents of the oceans and atmosphere as a result. First, so much dust is injected into the atmosphere ($\sim 1-2$ Pg per year at present) that it can cause changes in the amount of solar radiation scattered, absorbed or transmitted. Currently, it is thought that dust has a net cooling effect on the Earth's climate but when the dust contains significant concentrations of haematite, it tends to produce a warming effect, through absorption and re-radiation effects. Second, dust can also act as condensation nuclei in the atmosphere, resulting in changes in precipitation on regional scales. Third, iron-bearing dust can act to 'fertilize' areas of the world's oceans which are currently starved of iron, which reduces their biological productivity. Marine plankton need iron to grow but areas of the ocean which are remote from the dust-supplying continents (e.g. the Southern Ocean, the northern Pacific) are deficient in iron unless it is supplied to them by windblown dust. Modern experiments have shown that these ocean areas respond quickly and dramatically when they are artificially 'fertilized' with iron (e.g. [56]); the resulting bloom in plankton growth causes carbon dioxide to be drawn down into the ocean from the atmosphere, as the plankton use up increased amounts of carbon from the ocean water, some of which then sinks to the ocean floor as carbon-bearing sedimentary 'ooze'. During past glacial stages, the amount of dust blown into the atmosphere increased globally by between $2-5\times$. It is possible that dust-induced iron fertilization and atmospheric radiation changes may have played a key role in amplifying or modulating the orbitally-forced impacts on the Earth's climate in the past, and may do in the future. Magnetic methods are particularly suited to retrieving records of past dust flux from deep-sea sedimentary records, and identifying their iron oxide mineralogy (e.g. [19]). A key requirement is to obtain accurate past records of dust type, grain size and flux for a range of the low productivity ocean regions, but also to obtain precise dating of the sediments, in order to establish if the change in dust flux occurred before, during or after the change in ocean productivity and possible atmospheric change. This information is key because in models of future climate change, due to enhanced global warming, large changes in dust flux are predicted. Climate models currently cannot predict reliably whether these dust flux changes will result in cooling of the planet or additional warming.

Finally, within environmental magnetism, new measurement capabilities as well as new environmental issues are

also evolving. On the one hand, additional analytical techniques for improved characterization of whole samples are being developed, such as the use of first-order reversal curves to examine magnetic grain interactions or the magnetic properties of weakly magnetic haematite and goethite even when magnetite is dominantly present (e.g. [57,58]). On the other hand, examination and modelling of magnetic materials and processes at the nanoscale is also burgeoning, through use of atomic force microscopy and electron holography, and micro-magnetic modelling. Environmental magnetism will thus continue to grow, as it is applied to new and diverse fields; its methods and data processing develop to provide quantitative assessment of the magnetic components present in different environmental materials; and its users engage further with a diverse range of increasingly pressing environmental issues and model-testing.

Acknowledgements

I thank Ian Bradley for critical reading of the manuscript. This work has been supported by the Royal Society and by the Natural Environment Research Council (UK) and the Leverhulme Trust.

References

[1] J.R. Petit, J. Jouzel, D. Raynaud, *et al*., Nature **399** 429 (1999).
[2] U. Siegenthaler, T. Stocker, E. Monnin, *et al*., Science **310** 1313 (2005).
[3] L. Tauxe, *Lectures in Paleomagnetism*. Available online at: http://earthref.org/MAGIC/books/Tauxe/2005 (2005).
[4] D. Jiles, *Introduction to Magnetism and Magnetic Materials* (Chapman & Hall, London, 1998).
[5] R.F. Butler, *Paleomagnetism: Magnetic Domains to Geologic Terranes* (Blackwell Scientific Publications, Boston, 1992).
[6] P.H. Dankers, Magnetic properties of dispersed natural iron oxides of known grain sizes. PHD thesis, University of Utrecht (1978).
[7] B.A. Maher, R. Thompson and M.W. Hounslow, in *Quaternary Climates, Environments and Magnetism*, edited by B.A. Maher and R. Thompson (Cambridge University Press, Cambridge, 1999).
[8] B.A. Maher, Palaeogeogr. Palaeoclimatol. Palaeoecol. **137** 25 (1998).
[9] C.E. Mullins, J. Soil Sci. **28** 223 (1977).
[10] B.A. Maher and R.M. Taylor, Nature **336** 368 (1988).
[11] D.A. Bazylinski, Mat. Res. Soc. Symp. Proc. **218** 81 (1991).
[12] B.A. Maher and R. Thompson (Editors), *Quaternary Climates, Environments and Magnetism* (Cambridge University Press, Cambridge, 1999).
[13] R.P. Blakemore, Science **190** 377 (1975).
[14] J. Matzka and B.A. Maher, Atmos. Environ. **33** 4565 (1999).
[15] J.H. Puffer, E.W. Russell and M.R. Rampino, J. Sed. Petrol. **50** 247 (1980).
[16] I.F. Snowball, Phys Earth Planet. Int. **68** 32 (1991).
[17] A.P. Roberts, Earth Planet. Sci. Lett. **134** 227 (1995).
[18] Q. Liu, S.K. Banerjee, M.J. Jackson, *et al*., Geophys. Res. Lett. **29** 6-1-4 (2002).
[19] B.A. Maher, V.V. Karloukovski and T.J. Mutch, Earth Planet. Sci. Lett. **226** 491 (2004).
[20] Ö. Özdemir and S.K. Banerjee, Earth Planet Sci. Lett. **59** 393 (1982).
[21] B.A. Maher, Geophys. J. Roy. Astr. Soc. **94** 83 (1988).
[22] R. Thompson, Phys. Earth Planet. Inter. **42** 113 (1986).
[23] R. Egli, Stud. Geophys. Geodaet. **48** 391 (2004).
[24] D. Heslop and M. Dillon, Geophys. J. Int. **170**(2) 556 (2007).
[25] T. Von Dobeneck, Gesteinsmagnetizche Untersuchungen an tiefsee-sedimenten des Sudatlantiks. Diplomarbeit Inst. Allg. Angew. Geophys., Ludwig Maximilian University, München (1985).
[26] M.W. Hounslow and B.A. Maher, Geophys. J. Int. **124** 57 (1996).
[27] R.J. Harrison, R. Dunin-Borkowski and A. Putnis, Proc. Nat. Acad. Sci. **99** 16556 (2002).
[28] R.E. Dunin-Borkowski, M.R. McCartney and D.J. Smith, in *Encyclopedia of Nanoscience and Nanotechnology*, edited by H.S. Nalwa (American Scientific, Valencia, CA, 2004), pp. 41–100.
[29] F. Heller and T.S. Liu, Geophys. Res. Lett. **13** 1169 (1986).
[30] H. Zheng, F. Oldfield, L. Yu, *et al*., Phys. Earth Planet Int. **68** 250 (1991).
[31] B.A. Maher and R. Thompson, Geology **19** 3 (1991).
[32] F. Heller, X. Liu, T.S. Wu, *et al*., Earth Planet. Sci. Lett. **103** 301 (1991).
[33] Q.S. Liu, J. Torrent, B.A. Maher, *et al*., J. Geophys. Res. (Solid Earth) **110**(B11) art. no. B11102 (2005).
[34] R.A. Rosello-Mora, F. Caccavo, K. Osterlegner, *et al*., System. Appl. Microbiol. **17**(4) 569 (1995).
[35] B.A. Maher, A.O. Alekseeva and T. Alekseeva, Palaeogeogr. Palaeoclimatol. Palaeoecol. **201** 321 (2003).
[36] R. Thompson and B.A. Maher, Geophys. J. Int. **123** 611 (1995).
[37] B.A. Maher, R. Thompson and L.P. Zhou, Earth Planet. Sci. Lett. **125** 461 (1994).
[38] B.A. Maher and M. Hu, The Holocene **16** 309 (2006).
[39] C.G. Langereis and M.J. Dekkers, in *Quaternary Climates, Environments and Magnetism*, edited by B.A. Maher and R. Thompson (Cambridge University Press, Cambridge, 1999), pp. 352–382.
[40] J. Croll, Philos. Mag. **28** 121 (1864).
[41] M. Milankovitch, *Canon on Insolation and the Ice Age Problem* (Koninglich Serbische Academie, Belgrade, 1941), pp. 1–633.
[42] J.D. Hays, J. Imbrie and N.J. Shackleton, Science **194** 1121 (1976).
[43] A. Berger, M.F. Loutre and C. Tricot, J. Geophys. Res. **98** 10341 (1993).
[44] A. Berger and M.F. Loutre, Quaternary Sci. Rev. **10** 297 (1991).
[45] F.J. Hilgen, Earth Planet. Sci. Lett. **104** 226 (1991).
[46] J. Laskar, F. Loutel and F. Boudin, Astron. Astrophys. **270** 522 (1993).
[47] N.J. Shackleton, A. Berger and W. Peltier, Trans. Roy. Soc. Edin: Earth Sci. **81** 251 (1990).
[48] L. Tauxe, T. Herbert, N.J. Shackleton, *et al*., Earth Planet. Sci. Lett. **140** 133 (1996).
[49] P.R. Renne, A.L. Deino, R.C. Walter, *et al*., Geology **22** 783 (1994).
[50] Z. Ding, Z. Yu, N.W. Rutter, *et al*., Quaternary Sci. Rev. **13** 39 (1994).
[51] G. Bond, B. Kromer, J. Beer, *et al*., Science **294** 2130 (2001).
[52] M. Stuiver, T.F. Braziunas, P.M. Grottes, *et al*., Quaternary Res. **48** 259 (1997).
[53] S. Porter and Z.S. An, Nature **375** 305 (1995).
[54] F.D. Vine and D.H. Matthews, Nature **199** 947 (1963).
[55] S.J. Watkins, B.A. Maher and G.R. Bigg, Paleoceanography **22** PA2204 (2007) (DOI: 10.1029/2006PA001281).
[56] H.J.W. De Baar, P.W. Boyd, K.H. Coale, *et al*., J. Geophys. Res. **110** C09S16 (2005) (DOI: 10.1029/2004JC002601).
[57] C. Carvallo, O. Ozdemir and D.J. Dunlop, J. Geophys. Res. **109** art. no. B04105 (2004).
[58] A.R. Muxworthy, J.G. King, D. Heslop, *et al*., EOS Trans. AGU **84** Jt. Assem. Suppl. Abstract GP31B-0749 (2003).

Barbara Maher is a Professor within the Lancaster Environment Centre, University of Lancaster and presently holds a Royal Society-Wolfson Research Merit Award. She was awarded the Chree Medal by the Institute of Physics in 2005, for her 'pioneering contributions to the study of magnetic signals from the geological record as a means of determining climatic changes'. In addition to using environmental magnetism and palaeomagnetism to retrieve palaeoclimatic and dating information from sediments, she also applies magnetic methods to current environmental processes and problems, including: biomagnetic measurements of vehicle-derived particulate pollutants (of significant hazard to human health); tracing of modern fluvial sediment sources; and magnetic 'clean-up' of contaminated waters, using novel synthetic nanomagnetic materials. Her Centre for Environmental Magnetism and Palaeomagnetism is internationally acknowledged as a leading, innovative and agenda-setting research centre.